5-12-2021

Demonstration of Automated DNA Assembly on a Digital Microfluidic Device

Hee Tae An
hxa6018@rit.edu

ROCHESTER INSTITUTE OF TECHNOLOGY
ROCHESTER, NY

Demonstration of Automated DNA Assembly on a Digital Microfluidic Device

by

Hee Tae An

A Thesis Submitted in Partial Fulfillment of the Requirements for the Degree of
Master of Science in Microelectronic Engineering

Submitted May 12, 2021

DEPARTMENT OF ELECTRICAL AND MICROELECTRONIC ENGINEERING
KATE GLEASON COLLEGE OF ENGINEERING

Approved By:

Dr. Michael Schertzer, Associate Professor   Date
Thesis Advisor, Department of Mechanical Engineering

Dr. Karl Hirschman, Professor   Date
Committee Member, Department of Electrical and Microelectronic Engineering

---
Dr. Ivan Puchades, Assistant Professor   Date
Committee Member, Department of Electrical and Microelectronic Engineering

---
Dr. Michael Schrlau, Associate Professor   Date
Committee Member, Department of Mechanical Engineering

Dr. Sean Rommel, Director of Microelectronic Engineering/Professor   Date
Department Representative, Department of Electrical and Microelectronic Engineering

Abstract

The rapid manufacturing of highly accurate synthetic DNA is crucial for its use as a molecular tool, the understanding and engineering of regulatory elements, protein engineering, genetic refactoring, engineered genetic networks and metabolic pathways, and whole-genome syntheses [1,2]. Recent efforts in the development of enzyme mediated oligonucleotide synthesis have shown much potential to benefit conventional DNA synthesis [3–5]. With its success in applications as chemical microreactors [6–10], biological assays [8–14], and clinical diagnostic tools [10, 15–19], digital microfluidic (DMF) devices are an attractive platform to apply the promising benefits of enzymatic oligonucleotide synthesis to the manufacturing of synthetic DNA. This thesis work aims to demonstrate automated DNA assembly using oligonucleotides on a DMF device through the demonstration and validation of an automated DNA assembly protocol.

The prototyping process performed through this work revealed various important design considerations for the reliability of fluid handling performance and the mitigation of failure modes. To prevent dielectric breakdown or electrolysis, a relatively thick SU-8 3005 dielectric is used to remove the sensitivity of the device to variances in dielectric thickness and quality. To enable droplet creation, the gap distance between the DMF chip and top-plate is created and minimized using a thick SU-8 2100 layer. Reliable droplet creation is achieved through the use of electrode geometry that targets predictable fluid delivery and cutting. Reliable droplet transport is achieved through the use of a electrode interdigitation geometry that targets lower total electrode surface area and higher interdigitation contact area. The testing of DNA laden fluids revealed that biofouling can be a large concern for the demonstration of DNA assembly on a DMF device if droplets are moved through an air medium. To mitigate its effects, the final DMF device design featured the use of a permanently bonded top-plate with bored inlet/outlet ports as well as a silicone oil medium.

The final DMF device design was used to demonstrate automated DNA assembly. This demonstration involved the creation, transport, and mixing of DNA brick samples. These samples are subsequently incubated on a chemical bench or on the DMF chip to create recombinant DNA containing genetic information. DNA gel imaging of DNA assembly products from on-chip protocols compared to protocols performed on a chemical benchtop revealed comparable results. Through the course of this work, the applicability of automated DNA assembly on a DMF device was validated to provide preliminary results in the ultimate goal of DNA synthesis using enzymatic oligonucleotide synthesis.

Acknowledgments

I would first like to thank my advisor, Dr. Michael Schertzer. Since my first research opportunity as an undergraduate student in his lab, Dr. Schertzer has shown constant encouragement toward my curious disposition while ensuring that I was able to maintain my focus in reaching my research goals. Without his guidance and mentorship, this thesis work would have not have been possible.

The members of my committee, Dr. Karl Hirschman, Dr. Ivan Puchades, and Dr. Michael Schrlau, also deserve much acknowledgment for their assistance in ensuring this work would be able to meet the caliber of a master thesis. It is due to their efforts that this document is able to clearly illustrate the many contributions made throughout the course of this thesis work.

In addition, I would like to thank Dr. Lea Michel for her guidance with the DNA assembly through ligation protocol. With little experience with biochemistry and nucleic acids, the help of Dr. Michel and her research group was crucial in the understanding of as well as the acquisition of the necessary materials and equipment for the DNA assembly protocol and gel imaging.

The fabrication of the devices used in this work is made possible by the Semiconductor & Microsystems Fabrication Laboratory (SMFL). In particular, Thomas Grimsley, Patricia Meller, Sean O'Brien, and the many technicians that ensure the smooth operation of the SMFL, deserve much recognition for their constant support during design, fabrication, and failure analysis.

I would also like to acknowledge the faculty and staff of the Microelectronic Engineering department. It is because of their academic and administrative support that I was able to find the resolve to overcome the many challenges that I faced in the 7 years at RIT. In particular, I would like to thank Dr. Sean Rommel who has been a key mentor for my academic and professional success through all these years.

Table of Contents

List of Figures

List of Tables

1 Introduction

Digital microfluidic (DMF) devices commonly use electrowetting on dielectric (EWOD) to apply asymmetric electric fields to manipulate droplets [10, 20–22]. These devices have been used to automate chemical and biological processes at a microscopic scale by creating and individually manipulating discrete volumes of fluid [8, 9, 23]. Often referred to as a lab-on-a-chip (LOC) platforms, DMF devices have demonstrated much success in LOC applications as chemical microreactors [6–10], biological assays [8–14], and clinical diagnostic platforms [10, 15–19]. One LOC application that has the potential to benefit from DMF devices is the manufacturing of synthetic deoxyribonucleic acid (DNA).

DNA is comprised of a sequence of nitrogenous bases that governs the development, function, growth, and reproduction of living cells. The rapid manufacturing of highly accurate synthetic DNA is crucial for applications in synthetic biology such as: molecular tools, understanding and engineering regulatory elements, protein engineering, genetic refactoring, engineering genetic networks and metabolic pathways, whole-genome syntheses, and DNA nanotechnology [1, 2]. The manufacturing of custom sequences of synthetic DNA typically consists of two main processes: (1) the synthesis of short single stranded molecules called oligonucleotides and (2) the annealing and assembly of oligonucleotides into long chains of double stranded DNA [1, 24, 25].

While the amplification and assembly of DNA is done using a combination of various techniques, the synthesis of oligonucleotides is primarily done through a high-throughput process enabled by phosphoramidite chemistry [26, 27]. A limitation in this chemical process is its sensitivity to the presence of water. While it is required during the oxidation step, the presence of water causes decreased reactivity during the coupling step [28–30]. Because of this sensitivity to the presence of water, this chemistry relies on the use of an acetonitrile solvent to achieve high solubility of nucleoside carrying phosphoramidites as well as the accuracy and robustness of synthesis [31–33]. Because EWOD manipulation of acetonitrile has seen mixed success [7, 34–36], DMF devices have not previously been used as a platform for oligonucleotide and DNA synthesis.

Recent research efforts in enzyme mediated oligonucleotide synthesis has shown potential as a promising successor to phosphoramidite chemistry for oligonucleotide synthesis due to its improvements to strand length, error rate, throughput, and cost of production [3–5]. Among these improvements, a key advantage of enzymatic oligonucleotide synthesis is its ability to be performed using a water solvent [3, 4]. Because DNA assembly is typically conducted in water [1, 24, 37, 38], a new manufacturing scheme that integrates both oligonucleotide synthesis and DNA assembly on one platform has become possible.

Digital microfluidic (DMF) devices are an attractive platform to automate DNA synthesis. In comparison to continuous flow microfluidic platforms, DMF devices offer various advantages in its cost of manufacturing, flexibility in configuration, as well as the speed and efficiency in operation [9, 10, 23, 39]. By creating a device and manipulation scheme able to support the necessary fluid functions and chemistry, DMF devices may be able to complement the advantages offered by enzymatic oligonucleotide synthesis for the manufacturing synthetic DNA.

2   The Research Question

This thesis seeks to answer the question: Can digital microuidic devices be used to automate DNA assembly? Answering this research question is the first step toward integrating enzymatic oligonucleotide synthesis and DNA assembly on a single, disposable EWOD DMF device. If the current work is successful, it will pave the way for future work to implement enzymatic oligonucleotide synthesis in order to demonstrate the entire DNA synthesis process.

This thesis will answer the research question by (1) taking insight from published works to design and fabricate a suitable DMF device, (2) examining the compatibility of DNA laden droplets on those devices, and (3) demonstrating successful automated DNA assembly by comparing on-chip results to those from traditional benchtop methods.

3 Background & Theory

The primary goal of this thesis work is to develop a digital microfluidic (DMF) to automate DNA assembly. DMF devices perform fluid handling functions through the application of asymmetric electric field to manipulate droplets [20, 22, 40]. To understand how these devices work, we must understand how droplets typically wet surfaces and how that behavior can be manipulated by electrowetting.

3.1 Wetting

The shape of a fluid sitting on a surface is determined by the interaction of various forces such as gravity and surface tension [41–43]. Surface tension is the force that results from the balance of cohesive forces from each constituent phase state and adhesive forces from each interface in a system. As the size of a fluid approaches microscopic length scales, surface tension forces begin to dominate the influence of gravity to shape the fluid into a droplet [44, 45]. In this sense, gravity and surface tension compete to determine the shape of a fluid. The resultant shape of a microscopic droplet sitting on a surface can therefore be described as a spherical cap containing the surface tension forces within the system. This droplet shape is depicted in Figure 3.1.
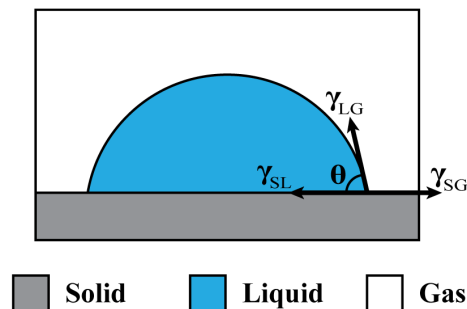
Figure 3.1: Illustration of a common droplet wetting scenario depicting a spherical cap which consists of the equilibrium contact angle θ resultant from the force balance of the solid-liquid γ_{SL}, liquid-gas γ_{LG}, and solid-gas γ_{SG} surface tensions that make up the triple contact line

3.1.1 Young's Equation

In the system seen in Figure 3.1, three interfaces exist: solid-liquid, liquid-gas, and solid-gas. This system is at equilibrium when the solid-liquid γ_{SL}, liquid-gas γ_{LG}, and solid-gas γ_{SG} surface tension forces are balanced. The resultant shape of the droplet from this force balance is commonly described by the contact angle [46–48]. A common method for relating the contact angle to the surface tension forces is through a mechanical force balance

$$\gamma_{LG}(\cos\theta) = \gamma_{SG} - \gamma_{SL}. \tag{1}$$

Equation (1) expresses the equilibrium condition where the vector sum of the surface tension forces are balanced as seen in Figure 3.1. The resultant angle between the solid-liquid γ_{SL} and liquid-gas γ_{LG} surface tension forces is known as the equilibrium contact angle θ. The line where this triple interface exists is known as the triple contact line. Equation (1) is often rearranged to describe the system through the equilibrium contact angle

$$\cos\theta = \frac{\gamma_{SG} - \gamma_{SL}}{\gamma_{LG}}. \tag{2}$$

The relationship shown in Equation (2) is known as Youngs equation [46] and can be used to describe the equilibrium contact angle of a droplet on a surface. If the fluid wetting a surface is small enough to be modeled as a spherical cap, the shape of the droplet can be estimated using the equilibrium contact angle and any other geometric parameter (e.g. volume, height, contact radius, radius of curvature, etc.). Surfaces and materials in wetting systems can be primarily described by this equilibrium contact angle. In short, a water droplet wetting a surface with an equilibrium contact angle below $90°$ would indicate a hydrophilic surface while greater angles would indicate a hydrophobic surface.

3.1.2 Contact Angle Hysteresis

Young's equation only concerns the basic thermodynamic relations to describe an system in static equilibrium [47, 49]. Due to this fact, factors such as surface roughness, heterogeneity, adsorption/desorption are not considered [50–53]. These non-ideal factors contribute to large variances in wetting behaviors of systems that consist of the same solid, liquid, and gas. The effects of these factors can be observed in Figure 3.2 where the measured contact angle of advancing and receding edges of a fluid in motion diverge from the equilibrium contact angle.

To account for these non-ideal factors, the measured static contact angle is referred to as the apparent contact angle. For a fluid in motion, the difference in advancing and receding contact angles is referred to as contact angle hysteresis. The measurement of these wetting characteristics are often used to describe degree of the random pinning forces and the relative wetting performance of the system [54–58].

The detection of this divergence of the apparent contact angle from equilibrium as well as the increase in contact angle hysteresis is an important consideration for the success of a DMF device. This is due to these effects being attributed to random pinning forces from surface roughness, heterogeneity, and adsorption/desorption. The origins and effects of these phenomenon is analyzed elsewhere [47, 50–53, 55, 57, 58]. Understanding the general role of random pinning forces, the DMF devices used in this work will attempt to mitigate its effects.
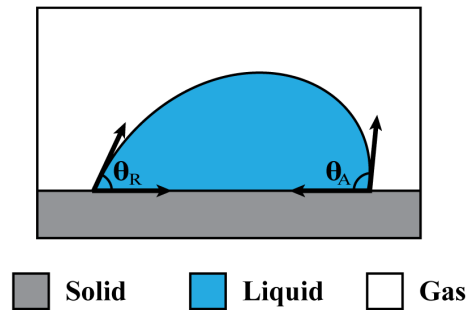
Figure 3.2: Example of contact angle hysteresis scenario in a mobile droplet depicting the apparent contact angles of the advancing θ_A and receding θ_R triple contact lines

3.2 Electrowetting on Dielectric

Electrowetting describes the modification of liquid wetting behavior through the interaction of an electrolyte or polar solvent with the induced charges on a conductive surface. By including a dielectric to the system, the induced charge density is enhanced. The processes involved in Figure 3.3 can be summarized through the following steps:

1. An electric field is applied between the droplet and conductor to accumulate charges on the conductor surface;

2. The accumulated conductor charge polarizes the dielectric and subsequently induces an accumulation of charge, ions, and dipoles in the droplet near dielectric surface;

3. The induced accumulation of charges, ions, and dipoles rearrange and spread the contact area between the droplet and dielectric interface; and

4. Static equilibrium is reached when the interfacial forces are balanced at the triple contact line between the droplet, dielectric, and medium.
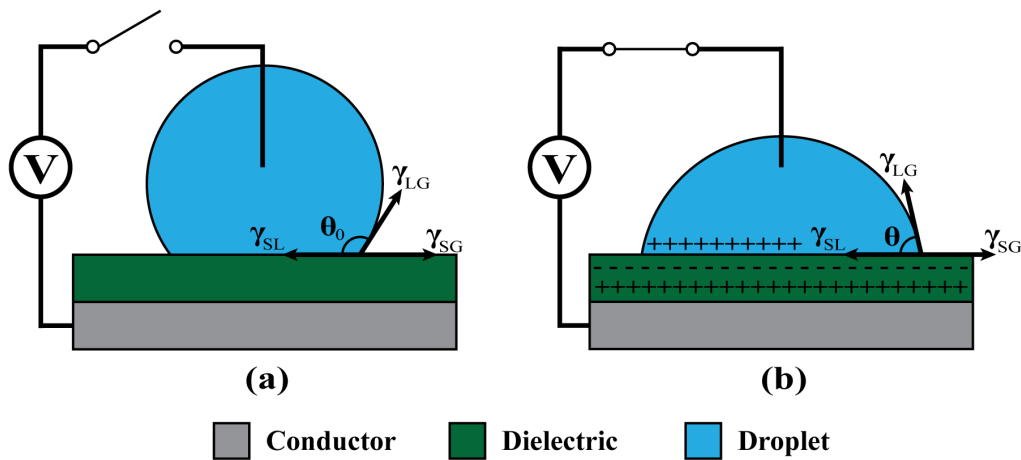
Figure 3.3: Illustration of electrowetting on dielectric depicting the modification of the apparent contact angle θ_0 to the electrowetting contact angle θ (a) before and (b) after the application of an electric field

7

3.2.1   Young-Lippmann Equation

The most common method for describing electowetting performance is through the analysis of the apparent contact angle of the droplet caused by the application of an electric field [59–62]. Applying an electric field to an EWOD system adds an electrowetting force to the force balance at triple contact line. Figure 3.3 depicts droplet profiles (a) before and (b) after the application of an electric to modify the apparent contact angle θ_0 to the electrowetting contact angle θ. To understand the effects of this induced electrowetting force, Young's equation must be revised. The contact line of a general EWOD system is represented in Figure 3.4 as a trapezoidal wedge that is displaced [54]. The following derivation summarizes the work conducted by Verheijen, Kang, and Mugele and Baret [54, 59, 63].

A droplet will spread in all directions until it has reached a minimum in free energy where γ_{SL}, γ_{LG}, γ_{SG} and the electrowetting force are balanced. With the addition of an applied potential, an electric charge density σ_L will be created in the liquid and induce an image charge density σ_S in the conductor to modify the force balance triple contact line as a resolution to the change in free energy of the system. This total change in the Helmholtz free energy dF of the system can be written as

$$dF = \gamma_{SL}dA - \gamma_{SG}dA + \gamma_{LG}dA\cos\theta + dU - dW_B \qquad (3)$$

where dA is the change in contact area between the solid/liquid interface, dU is the stored potential energy from the electric field created between the electrical charge densities, and dW_B is the work done by the voltage source to redistribute the created charge densities. Throughout this derivation, it is assumed that the system is in equilibrium at a constant potential V and that mechanisms for every dissipation are negligible.
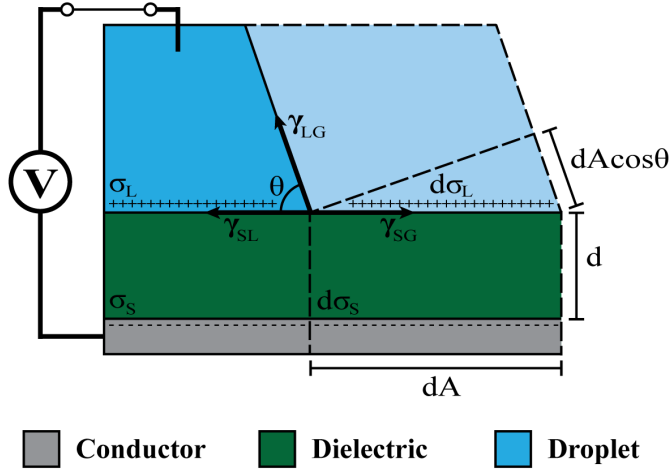
Figure 3.4: Representation of EWOD system as a trapezoidal wedge and the displacement of the triple contact line by dA

By first considering the case where there is no applied potential, it is understood that $dU = dW_B = 0$. At steady state, the free energy of the system is unchanged and therefore, $dF/dA = 0$. With this understanding, Equation (3) can be rewritten in the form of the Young's Equation to describe the contact angle with no applied potential θ_0:

$$\cos\theta = \frac{\gamma_{SG} - \gamma_{SL}}{\gamma_{LG}} = \cos\theta_0 \tag{4}$$

In the case with a nonzero applied potential, the potential energy resultant from the created charge densities must be included. The electrostatic potential energy per unit area in the EWOD system can be represented by

$$\frac{U}{A} = \int_0^d \frac{1}{2}\vec{E}\vec{D}dz \tag{5}$$

9

where $\vec{E}$ is the electric field, $\vec{D}$ is the displacement field, z is perpendicular to the surface, and d is the thickness of the dielectric layer. With the assumption that these charge distributions create a perfect parallel plate capacitor at a potential V, $\vec{E} = \frac{V}{d}$ and $\vec{D} = \sigma_L$. The change in the electrostatic potential energy as a function of the change in the contact area can be as:

$$\frac{dU}{dA} = \frac{1}{2}dED = \frac{1}{2}V\sigma_L \tag{6}$$

In addition to the electrostatic potential energy, the voltage source performs work to redistribute the created charge distribution. This work can be represented by

$$\frac{dW}{dA} = V\sigma_L \tag{7}$$

By substituting Equation (6) and (7) along with Gauss's Law ($\sigma_L = \epsilon_0\epsilon_r V/d$) into Equation (3) at a steady state where $dF/dA = 0$, the following equation can be derived:

$$\cos\theta = \frac{\gamma_{SG} - \gamma_{SL}}{\gamma_{LG}} + \frac{\epsilon_0\epsilon_r}{2d\gamma_{LG}}V^2 \tag{8}$$

Finally combining Equation (4) and (8) the Young-Lippmann or electrowetting equation is derived in order to describe the electrowetting contact angle as a function of the apparent contact angle and the applied potential:

$$\cos\theta = \cos\theta_0 + \frac{\epsilon_0\epsilon_r}{2d\gamma_{LG}}V^2 \tag{9}$$

The Young-Lippmann equation is a powerful tool in the analysis of the potential of EWOD performance with its ability to describe the wetting behavior of the system in terms of material dependent characteristics such as $\cos\theta_0$, ϵ_r, d, and γ_{LG} as well as device control parameters such as V. Using this equation, a DMF device can be designed to ensure the success of fluid handling functions through EWOD.

3.2.2 Contact Angle Saturation

Because the Young-Lippmann equation is derived from the original work by Young, this equation again only concerns the basic thermodynamic relations to describe a system in static equilibrium. In reality, increasing the applied voltage does not decrease the contact angle at the rate described by the Young-Lippmann equation [59, 61, 64–66]. This phenomenon is referred to as contact angle saturation and is depicted in Figure 3.5.

The detection of contact angle saturation is an important consideration for the success of a EWOD DMF device. Beyond the point of saturation, additional applied potential would not be able to further change the contact angle and therefore provide no benefits to droplet manipulation. Additionally, without the detection of contact angle saturation, the applied potential could eventually cause permanent breakdown of the dielectric and fluid. While the exact origin of contact angle saturation is not yet fully understood, several works have hypothesized that the effects may be due to charge leakage, dielectric charge trapping, contact line charge repulsion [67–69]. Though this work does not attempt to model contact angle saturation [63, 64, 70], the DMF devices used in this work will attempt to prevent the occurrence of breakdown.
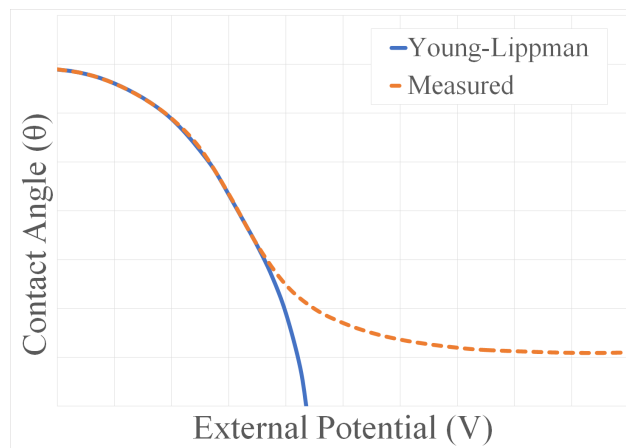
Figure 3.5: Effects of contact angle saturation depicting the theoretical Young-Lippman electrowetting equation and experimentally measured contact angles θ as a function of the applied external potential V

3.3 Digital Microfluidics

Microfluidics refers to devices and methods for controlling and manipulating fluid flows at a microscopic scale. Driven by efforts to create micro total analysis or lab-on-a-chip (LOC) systems [71], these devices primarily consist of a continuous flow configuration where fluid channels are fabricated on an inexpensive substrate and commonly driven through the use of a system of external mechanical pumps and valves. While they have seen much success in performing various physical, chemical, and biological processes [72], continuous microfluidic devices are limited as a complete LOC system due to its lack of reconfigurability, potential for cross-contamination, and trade-off between throughput and control complexity [39].

Digital microfluidics (DMF) in contrast refers to devices and methods for controlling and manipulating discrete volumes of fluid in the form of a droplet. The most common method for droplet manipulation is electrowetting on dielectric (EWOD). EWOD DMF devices are primarily constructed using (a) a chip comprised of a two-dimensional array of electrodes covered in a dielectric and hydrophobic coating that is encapsulated by (b) a top-plate comprised of a transparent grounding electrode covered in a hydrophobic coating.

In contrast to the general EWOD device that use an open configuration, DMF devices use asymmetric electric fields on confined droplets to perform the manipulations necessary for various fluid handling functions. As seen in Figure 3.6, this process consists of the use of electrowetting to selectively modify the wetting behavior of the contact line in specific directions.

With the inclusion of this selective directionality, EWOD DMF devices are able to integrate key fluid handling functions to create, transport, and mix droplet samples to enable a higher level flexibility as a complete LOC system [10]. By integrating of these key functions, EWOD DMF devices are able to provide numerous advantages LOC system [9, 10, 19, 39]:
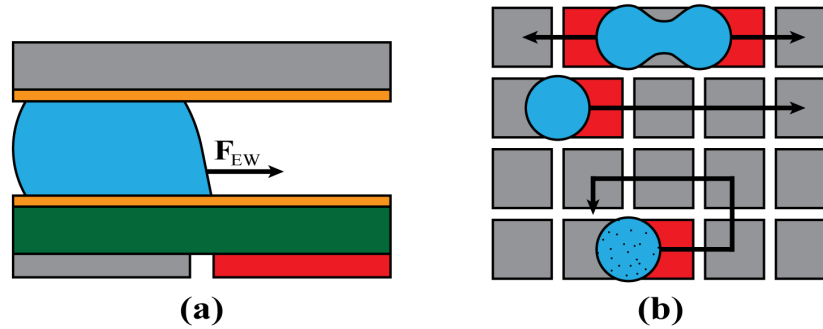
Figure 3.6: Depiction of (a) asymmetric electrowetting on a DMF device and (b) splitting, transport, and mixing fluid handling functions

- High speed manipulation

- Compatibility with many electrolyte solutions

- Compatibility with optical and capacitive sensing for process monitoring

- Minimization of droplet evaporation through the use of a fluid medium

- Lack of mechanical parts that may fail

- Lack of microfabricated channels that increase design complexity and costs

- Lack of direct currents that cause undesired heating and reactions

With these advantages, DMF devices have demonstrated success in LOC applications as chemical microreactors [6–10], biological assays [8–14], and clinical diagnostic platforms [10, 15–19]. While the potential of EWOD DMF devices as a LOC system is promising, it is important understand the governing principles that enable the droplet creation and transport functions. With numerous works focusing on modeling droplet dynamics [21, 73–78], the following sections will provide an overview of the droplet transport models from Ren et al. [73] and creation models from Cho et al. [10] that focus on important device design considerations that ensure the success of DNA assembly.

3.3.1 Droplet Transport

Droplet transport is the basis for all droplet handling on a DMF device. To ensure reliable operation of the device, it is important to understand the factors that affect its performance. In an EWOD device, an electric field is applied between the droplet and conductor. Electrowetting will increase the contact area between the droplet and dielectric until the interfacial forces are balanced at the triple contact line [21, 54, 59, 63]. In the case of DMF devices, the conductor is separated into a two-dimensional array of electrodes. As seen in Figure 3.7, an electric field is applied to an adjacent electrode in order to induce the accumulation of charge, ions, and dipoles only in the direction of this adjacent electrode [40, 79].

Ren et al. describes the instantaneous force created in this direction as an electrowetting force is created which persists until the droplet is transported to cover this adjacent electrode to balance the interfacial forces at the triple contact line [73]. By applying this electric field in a step wise manner, droplets can be simultaneously transported among the two-dimensional array of electrodes to perform multiple processes in parallel. The basic one-dimensional force generated from electrowetting F_{EW} can be determined by reorganizing the Young-Lippmann equation or Equation (9).

$$F_{EW} = \gamma_{LG}(\cos\theta - \cos\theta_0) = \frac{\epsilon_0\epsilon_r}{2d}V^2 \tag{10}$$
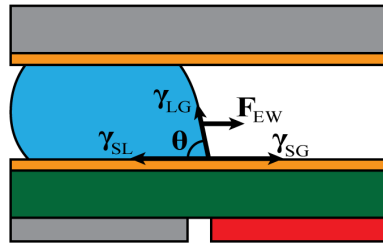
Figure 3.7: Illustration of triple contact line during droplet transport depicting the addition of an electrowetting force F_{EW}

14

Equation (10) depicts the electrowetting force in terms of the liquid-gas surface tension force γ_{LG} scaled by the difference in the electrowetting contact angle θ and the apparent contact angle θ_0 as a function of the vacuum permittivity ϵ_0, relative permittivity of the dielectric ϵ_r, thickness of the dielectric d, and the applied potential V. It is clear from this description that the electrowetting force can be increased through several methods: maximize γ_{LG} through droplet liquid and medium material selections, minimize θ and maximize θ_0 through the choice of surface material selection, maximize ϵ_r through dielectric material selection, minimize d during device fabrication, and maximize V during device operation.

While it does not account for energy dissipative and frictional forces from factors such as contact angle hysteresis or saturation [59, 63], Equation (10) does serve as a basic framework for successful droplet transport. With this understanding, the DMF device can be designed within the constraints of the available materials and manufacturing costs to ensure functionality for LOC applications.

Another key consideration for droplet transport is electrode geometry. Because EWOD relies on Coulombic attraction, the layout and design of transport electrode design therefore must be able to maintain a minimal separation. While the separation can be minimized through general microfabrication techniques, various groups have instead attempted to optimize the transport electrode geometry. The strategies used include the use of various electrode shapes [80–82], interdigitation of electrode edges [80, 82, 83], and the reduction of electrode surface area [80–83]. This work will attempt to use a combination of these various strategies to achieve reliable droplet transport performance.

3.3.2 Droplet Creation

The integration of the droplet creation function enables LOC protocols to be performed on DMF devices. To ensure reliable demonstration of these protocols, it is important to understand the factors that affect its performance. Droplet creation is enabled through the use of the top-plate to create hydrodynamic instability [21, 23, 39, 84–86]. As seen in Figure 3.8, droplets are created by splitting a large volume fluid through the use of three electrodes.

In this scenario, potential is applied to two end electrodes while the middle cutting electrode is left grounded. Upon actuation, the triple contact line at both ends are pulled in opposite directions. With continued contact line displacement, a pressure difference is created to cause the center of the fluid to neck. With a sufficiently large enough pressure difference, the fluid is split into two droplets.
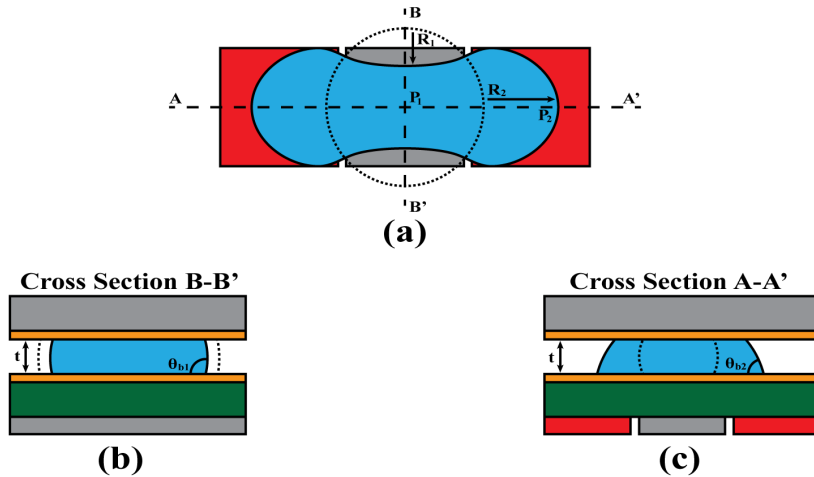
Figure 3.8: Illustration of droplet splitting depicting the (a) top down, (b) longitudinal, and (c) latitudinal cross sectional areas of the fluid

Various groups have attempted to model the criterion for splitting droplets in a DMF system [55,75,77,86,87]. Cho et al. examines the reliance of droplet creation on hydrodynamic instability by considering the pressure difference created between the two ends and center of the fluid column [83]. When the electrowetting force is applied to stretch the fluid column to the point of necking, the induced pressure difference can be related to the difference in contact angles $\cos\theta_{b2} - \cos\theta_{b1}$ and the respective radii of displacement R_1 and R_2 of the two regions

$$P_1 - P_2 = \gamma_{LG}\left(\frac{1}{R_1} - \frac{1}{R_2} + \frac{\cos\theta_{b2} - \cos\theta_{b1}}{t}\right) \tag{11}$$

where γ_{LG} is the liquid-gas surface tension and t is the channel gap within the DMF device. At static equilibrium where no necking occurs, the pressure of the two regions are equal. With this understanding, Equation (11) can be rewritten as the following:

$$\frac{R_2}{R_1} = 1 - \frac{R_2}{t}\left(\cos\theta_{b2} - \cos\theta_{b1}\right) \tag{12}$$

Understanding that the ends of the fluid column are undergoing electrowetting while the center is not, it can be assumed that the difference between $\cos\theta_{b2}$ and $\cos\theta_{b1}$ is the same as the relationship described in the Young-Lippmann equation or Equation (9). Equation (12) can therefore be rewritten as the following:

$$\frac{1}{R_1} = \frac{1}{R_2} - \left(\frac{1}{t}\right)\frac{\epsilon_0\epsilon_r}{2d\gamma_{LG}}V^2 \tag{13}$$

Equation (13) provides key insight into the necessary factors for the successful creation of a droplet. Necking is initiated when R_1 becomes non-zero and negative. This condition can be satisfied through a variety of methods: increase R_2 continued displacement of the ends of the fluid column, decrease t nad d during device fabrication, increase ϵ_r through dielectric choice, and increase V during device operation. While it does not account for the effects of contact angle hysteresis [50–53, 55, 57, 58] or saturation [63, 64, 70], Equation (13) is able to clearly represent the reliance of droplet creation on both geometric factors and EWOD.

Even when the criterion in Equation (13) is met, a common issue that occurs during the droplet creation process is non-uniform splitting [39]. This issue is caused by a necking region that is created off center in the cutting electrode. Various groups have attempt to address this issue through the use of various creation electrode geometries [87, 88]. The strategies used include the use of a modified cutting electrode geometry or off-center displacements of the contact line during EWOD. This work will attempt to use a combination of these strategies to achieve reliable droplet creation performance.

3.3.3 Biofouling

A general issue for microfluidic devices that perform biological protocols is biofouling [89–92]. Biofouling concerns the adsorption and accumulation of biological materials onto the active surfaces of the device. General mechanisms that contribute to biofouling are surface roughness, electrostatic interaction, and van der Waals forces [93, 94]. Because these devices rely on surface tension to drive fluid manipulation, surface fouling can greatly contribute to random pinning points and eventual device failure. The issue of biofouling is addressed using various strategies: surface structure engineering [95, 96], antifouling surface or bulk materials [97, 98], surfactant additives [99], lubricant additives [100], and a combination of these strategies [101]. This work will attempt to use a combination of these various strategies to mitigate observed biofouling.

18

3.4 DNA Synthesis

To put this thesis work into context it is necessary to understand the details regarding DNA synthesis. The rapid manufacturing of synthetic DNA relies on the use of short single-stranded chains of nucleobases called oligonucleotides [102]. Oligonucleotides are primarily synthesized using nucleoside phosphoramidite chemistry. This chemistry relies on the use of a protecting group to enable and disable the synthesis process. By performing subsequent DNA amplification and assembly, this conventional process has paved the way for the automation of high-throughput DNA synthesis [2]. With growing demands high strand length and throughput with low error rates and cost of production cost, the limits of phosphoramidite chemistry poses on the manufacturing of DNA is becoming more apparent [1].

Recent research efforts to address the length, cost, and throughput limits of the phosphoramidite method have seen a large push for the use of enzymatic oligonucleotide synthesis [3–5]. Figure 3.9 summarizes the difference between the conventional phosphoramidite (Figure 3.9a) and the enzyme mediated oligonucleotide synthesis process (Figure 3.9b).
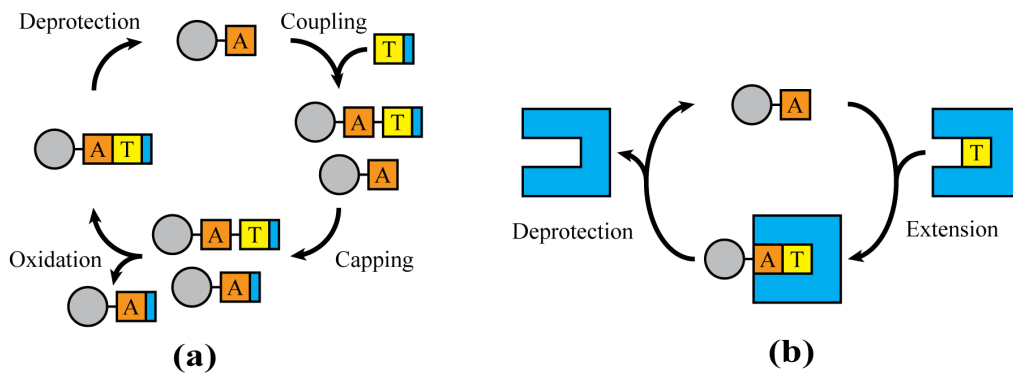
Figure 3.9: Example of (a) conventional oligonucleotide synthesis and (b) enzyme mediated oligonucleotide synthesis

Enzymatic oligonucleotide synthesis is an attractive alternative over the phosphoramidite method due to its robustness of enzymes, potential for process optimization through enzyme engineering, ability to initiate synthesis from natural DNA [3]. The crucial element that makes this process an attractive candidate for EWOD DMF devices is its ability to be performed in an aqueous medium [4, 5]. With previous success in DNA-based applications such as the purification and extraction of DNA samples, DNA hybridization assays, polymerase chain reaction, and pyro sequencing [10], DMF devices are a promising platform to complement the potential benefits of enzymatic DNA synthesis.

Synthesized oligonucleotides are transformed into DNA molecules through anneal and assembly processes [103–105]. Figure 3.10 summarizes the complete DNA synthesis process. These processes rely on Watson-Crick base pairing (guanine-cytosine and adenine-thymine) to form DNA molecules. Complementary strands of oligonucleotides are first annealed to form short DNA fragments with single strand overhangs (Figure 3.10a-b). To form long DNA products, DNA fragments are assembled using complementary single strand overhangs and a ligase enzyme (Figure 3.10b-c). This work will attempt to perform DNA assembly on a DMF device using bench annealed oligonucleotides. This preliminary work will be able to validate the compatibility of DMF devices for a DNA synthesis protocol that implements both the oligonucleotide synthesis and DNA assembly process.
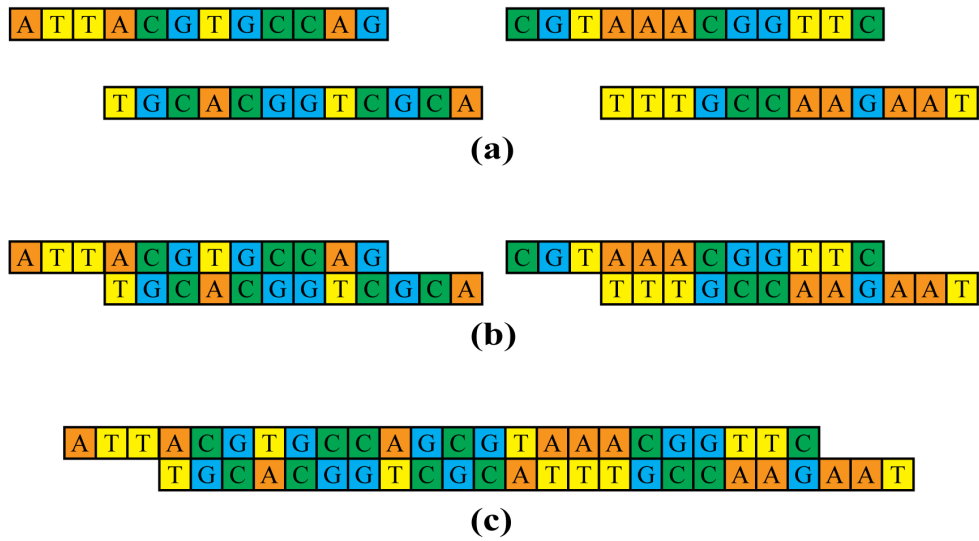
Figure 3.10: Example of complete DNA synthesis process that uses (a) oligonucleotide samples that are (b) annealed into DNA fragments and (c) assembled into DNA products

4 Experimental Methodology

The following sections outline the experimental methodology used for the demonstration of DNA assembly on a DMF device. The various materials, processes, and tools used in the design, fabrication, and testing of the DMF device will be described.

4.1 Device Design & Fabrication

The layout and design of the DMF device was key for reliable droplet creation and transport. To achieve this goal, an iterative process of device design, fabrication, and testing was used. In general, the DMF device layouts were designed in Adobe Illustrator or KLayout. These devices used an array of contact pads that were connected to the corresponding transport and reservoir electrodes. Electrodes designs took insight from the previous work of others. In general, key design considerations included electrode geometry and method of interdigitation. Device layouts maintained a minimum of 30 um line and 20 um space dimensions to ensure successful device fabrication. DMF device fabrication was conducted using conventional techniques in the Semiconductor & Microsystems Fabrication Laboratory (SMFL).

4.1.1 Air Medium DMF Prototype

DMF prototypes were all tested with an air medium. DMF prototype chips were fabricated on a bare 100 mm Eagle XG (Corning) wafer as the starting substrate (Figure 4.11a-i). Device wafers were first prepared by performing a piranha etch process. The aluminum electrode layer was sputter deposited onto each wafer (Figure 4.11a-ii). OiR 620 10 (Fujifilm) i-line photoresist was spin coated onto each wafer before performing contact lithography with a high-resolution transparency photomask. Each following lithography process was conducted using a similar photomask and process. The electrode pattern was transferred to the aluminum layer using an alu-

22

minum wet etch (Fujifilm) (Figure 4.11a-iii). A silicon dioxide dielectric layer was then deposited through chemical vapor deposition (Figure 4.11a-iv). OiR 620 10 photoresist was spin coated and patterned using contact lithography to be used as a contact cut mask. The silicon dioxide dielectric layer was patterned using a 16:3:3 pad etch (Fujifilm) (Fujifilm) (Figure 4.11a-v). Each wafer was then coated with OiR 620 10 photoresist to protect the surface. DMF chips were then diced from each wafer. After the protective OiR 620 10 photoresist was stripped, a polyimide adhesive (Kapton) was to mask the contact pads. A 50 nm hydrophobic layer of a diluted Teflon AF solution (Chemours) was then spin coated on the surface of each chip (Figure 4.11a-vi). In order to ensure that contact pads remained undamaged, the polyimide adhesive was left on the chips until it was time to encapsulate the devices.
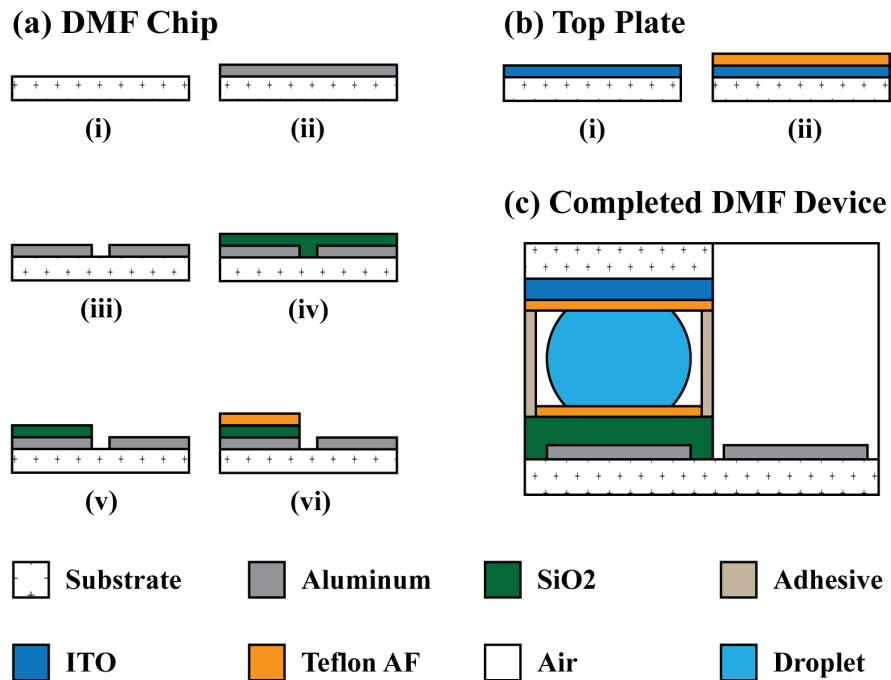
Figure 4.11: Microfabrication process flow depicting (a) prototype DMF chip, (b) top plate, and (c) the completed device

Device top-plates were fabricated using starting substrates consisting of 50 x 75 mm microscope slides with a 200 nm film of Indium Tin Oxide (Delta Technologies) (Figure 4.11b-i). Each top-plate used a polyimide adhesive to mask the corners of the top-plate. A 50 nm hydrophobic layer of a diluted Teflon AF solution was then spin coated on the surface of each top-plate (Figure 4.11b-ii). In order to ensure that contact areas remained undamaged, the polyimide adhesive was left on the top-plate until it was time enclose the devices for testing. The DMF chip and top plate were then bonded to form a completed DMF device. DMF device prototypes loaded the test fluid on to the reservoir electrodes and used a double-sided adhesive to bond the chip to the top plate. A copper adhesive was used to provide electrical contact to the uncoated corners of the top-plate. An example cross section of a completed device can be seen in (Figure 4.11c).

4.1.2   Oil Medium Final DMF Device

The final DMF device chips were fabricated on 50 x 75 mm microscope slides with a 100 nm aluminum film (Deposition Research Laboratory Inc.) as the starting substrate (Figure 4.12a-i). Each chip was first surface treated using a mild oxygen plasma and dehydration bake prior to the spin coating of an AZ MIR 701 i-line photoresist (Merck). Each following surface treatment was conducted using the same process. The electrode layer was patterned using contact lithography with a high-resolution transparency photomask. Each following lithography process was conducted using a similar photomask and process. The electrode layer pattern was transferred to the aluminum layer using an aluminum wet etch (Figure 4.12a-ii). Each chip was then again surface treated prior to the spin coating of SU-8 3005 negative photoresist (Microchem) that is used as the device dielectric. The SU-8 3005 dielectric was patterned using contact lithography (Figure 4.12a-iii). For the final DMF device chip, an SU-8 2100 negative photoresist (Microchem) was used as the gap and gasket template. The SU-8 2100 was spin coated and subsequently patterned using contact lithography (Figure 4.12a-iv). Each chip was then again surface treated prior to the use of a polyimide adhesive to mask the contact pads. A 50 nm hydrophobic layer of a diluted Teflon AF solution was then spin coated on the surface of each chip (Figure 4.12e) (Figure 4.12a-v). In order to ensure that contact pads remained undamaged, the polyimide adhesive was left on the chips until it was time to encapsulate the devices.

25
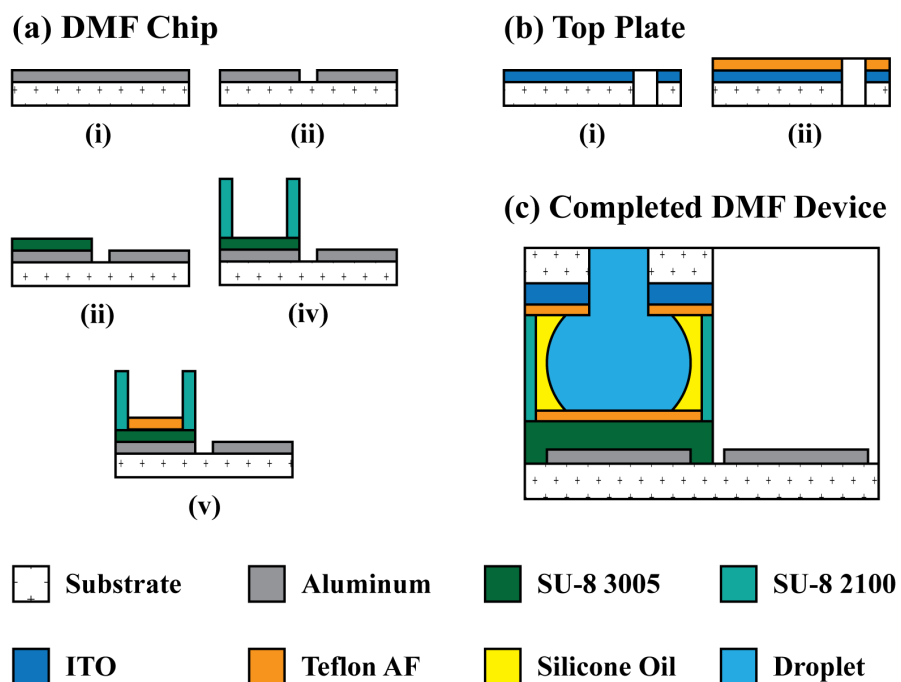
Figure 4.12: Microfabrication process flow depicting (a) final DMF chip, (b) top plate, and (c) the completed device

Device top-plates were fabricated using starting substrates consisting of 50 x 50 mm microscope slides with a 200 nm film of Indium Tin Oxide (Delta Technologies). The surface of the ITO was covered using a polyimide adhesive before a series of ten 1 mm inlet/outlet ports were bored using a CNC drill. (Figure 4.12b-i). After removing this adhesive, the corners of the each top-plate was masked using polyimide adhesive. A 50 nm hydrophobic layer of a diluted Teflon AF solution was then spin coated on the surface of each top-plate (Figure 4.12b-ii). In order to ensure that contact areas remained undamaged, the polyimide adhesive was left on the top-plate until it was time enclose the devices for testing. DMF chip and top plates were bonded to form a completed DMF device. The final DMF device design used a two part epoxy along the SU-8 2100 gap and gasket template. A copper adhesive was used to provide electrical contact to the top-plate. An example cross section of a completed device can be seen in (Figure 4.12c). Encapsulated devices were filled with 10 cSt silicone oil prior to testing. This was done by filling the device using an Eppendorf variable micropipette while covering all but two inlet/outlet ports.

26

4.2 Device Testing

4.2.1 Control Systems

Through the course of this work, two control systems were used to test DMF devices: a custom National Instruments control system and SciBots Dropbot system. The custom control system is a modular system that consists of various components that are controlled by the Lab-VIEW software. The DropBot system is a fully integrated system controlled by the MicroDrop software.

DMF devices during the prototyping process were tested using the custom control system. The control system consisted of a NI PXI 1033 chassis containing a NI PXI 5402 signal generator, NI PXI 4072 LCR multimeter, and NI PXI 2529 matrix switching card along with a Trek PZT700A Amplifier. During testing, a sinusoidal actuation signal was generated, amplified, and input into the matrix switching card and subsequently output into the 32 outputs of a custom 3D printed fixture.

DMF devices were controlled through the use of a custom virtual instrument (VI) in Lab-VIEW software. By interfacing with the NI PXI 1033 chassis, this VI was able to quickly change important parameters for DMF device operation. These parameters include: switch matrix location, signal amplitude, signal frequency, transport actuation duration, and creation actuation duration. In addition, this VI was able to quickly import simple protocols written in CSV format denoting the step number, switch matrix location, and actuation state. The custom control system was used to attempt both manual and automated droplet transport and creation. Videos of testing attempts were captured using a separate system that consists of a Point Grey Camera and a Zeiss SteREO Fluorescent Microscope. Videos were analyzed for modes of failure and used to create changes to the DMF device prototype.

Testing of the final DMF device design was conducted on the DropBot system. The DropBot system was chosen as a successor to the custom control system due to its robust hardware and software with features for troubleshooting, diagnostics, and performance monitoring. Prior to each automated protocol, a test PCB provided by Sci-Bots was used with the on-board diagnostics tests of the MicroDrop software to verify the functionality of the DropBot system. A DMF device was subsequently loaded onto system and tested using DI water and the realtime programming function of the Microdrop software. This was done in order to verify connection between system pins and DMF device pin pads. A webcam included in the DropBot control system was used to observe the DMF device during testing.

4.2.2   DNA Assembly

DNA laden droplets in this work used six oligonucleotides with a length of around 80 nucleotides (Integrated DNA Technologies). These oligonucleotides will be referred as 1A, 1B, 1C, 2A, 2B, and 2C. All oligonucleotides were 5'-phosphorylated with the exception of 1A, which is labeled with a 5'-Cy3 fluorophore. The sequences of these oligonucleotdes can be seen in Table 1. In this work, oligonucleotides 1A, 1B, and 1C were hybridized to form DNA Brick 1, and 2A, 2B, and 2C hybridize to form DNA Brick 2. These oligonucleotides (5 uM strand concentration) were annealed without ligation at 85 °C for 5 min in 1 x T4 DNA ligase buffer (New England Biolabs) and snap cooled on ice for 30 min. The following reagents were mixed using the following proportions to create working stock solutions of DNA Brick 1 and DNA Brick 2: 10 uL nuclease-free water, 0.6 uL of 10x T4 DNA ligase buffer (New England BioLabs), 0.1 uL of T4 DNA ligase (Thermo Fisher Scientific) and either 4.0 uL of solution containing DNA Brick 1 or 4.1 uL of solution containing DNA Brick 2. DNA assembly was conducted using Brick 1 and Brick 2 solutions. The two solutions were mixed on a chemical bench or on DMF devices and subsequently incubated at room temperature for a minimum of 10 minutes. Proteinase K and calcium chloride were then added to the mixture and incubated for 30 minutes at 37 °C then 10 minutes at 70 °C.

Table 1: Summary of oligonucleotide sequences

Name	Sequence (5'-3')
1A	/5Cy3/ATCGATTCTTTCTGCGGACCATGTTGT TCTGATACTTTGGTCATATTTCCGTTGTAGG AGTGAATTCACTTAGCTTTGCG
1B	/5Phos/AAGTGGTGTTCAGTTCGGTAACGGAG AATCTATGCGGCATTCTTATTAATACATTTGA AACACGCCCAATTGATACTAAA
1C	/5Phos/ATGCCGCATAGATTCTCCGTTACCGAA CTGAACACCACTTCGCAAAGCTAAGTGAAT TCACTCCTACAACGGAAATATGA
2A	/5Phos/TATCAAAGCTTGCTACCAATAATTAGC ATTATTGCCTTGCTGAACGTCGCGTGCGTAC ACTTTAATCTCCGGTTCAAGCT
2B	/5Phos/GCAAGGCAATAATGCTAATTATTGGTA GCAAGCTTTGATATTTAGTATCAATTGGGCG TGTTTCAAATGTATTAATAAGA
2C	/5Phos/GCAGTGTAGGTGTATCAATATAGCATG TAGCCACATCCTTAGCTTGAACCGGAGATT AAAGTGTACGCACGCGACGTTCA

Gel electrophoresis using an agarose gel (2% w/v) was used to image the results of DNA assembly through ligation. 1 g of agarose powder and 50 mL of 1X TAE buffer were mixed in a medium size beaker. This solution was heated in a microwave in increments of 30 s until clear in appearance and left to cool. After becoming cool enough to handle, 2 uL of ethidium bromide was added to the solution. The gel solution was then poured into the middle platform of an electrophoresis rig. The comb from the rig was then added to create the wells for each sample. The solution was left to dry for 30 min until the gel forms. After the comb is removed, the electrophoresis rig was filled with 1X TAE buffer until the surface of the gel is adequately covered. 1 uL of each DNA sample solution was pipetted into each well.

The ends of the electrophoresis rig was then connected to a power supply and run at 90 V for 50 minutes. Gel results were visualized using a ChemiDoc XRS+ imager (Bio-Rad). DNA is negatively charged and therefore reacts to an electric field. The effects of this electric field are impeded as DNA molecules grow in size. The base pairs lengths of a DNA sample can therefore be estimated through the use of a reference ladder that contains samples with equal increments of base pairs. Successful assembly in this work was validated through the use of a DNA reference ladder with 50 base pair increments to compare samples of DNA brick 1, DNA brick 2, and the assembled DNA from each protocol.

4.2.3 Experimental Procedure

The final DMF device in this work must be able to demonstrate a successful DNA assembly process. This DMF device must first be able to successfully demonstrate the necessary fluid handling functions of droplet transport and creation. The DMF device must then be assessed for any failure modes concerning DNA laden droplets. To achieve these larger aims, DMF device prototypes aim to achieve the following protocols:

1. Manual transport of DI water between two electrodes;

2. Manual creation of DI water droplet from the reservoir; and

3. Automated creation, transport, and mixing of DI water droplets.

The success of each protocol was validated when failure modes were not observed. With successful demonstration of the above protocols, the insight gained was used to create a final DMF device design supported by the DropBot system. This final design was then used to perform an automated DNA assembly protocol. This protocol used DNA Brick 1 and Brick 2 solutions to create two droplets which were transported and mixed together until extraction from the DMF device. The success of each protocol was validated through the examination of gel electrophoresis results. Because it is unclear if these DMF devices were compatible with the reagents especially at high incubation duration and temperatures, devices were tested incrementally as such:

1. Automated creation, transport, and mixing of DNA droplets, off chip incubation;

2. Automated creation, transport, and mixing of DNA droplets with extended exposure, off chip incubation; and

3. Automated creation, transport, and mixing of DNA droplets and incubation.

5 Results & Discussion

5.1 Device Prototyping

The first aim of this work was to validate a device design and fabrication method for a general DMF device. This was an iterative process that began with the fabrication methodology used in Schertzer et al. [78, 106]. To achieve a device suitable for DNA assembly, this aim is subdivided into the following aims: (a) droplet transport and (b) droplet creation.

5.1.1 Manual and Automated Droplet Transport

The demonstration of manual droplet transport was the first goal attempted on DMF prototype 1. The DMF device layout can be seen in (Figure 5.13). This design consisted 1 x 1 mm transport electrodes based on the work of Pollack et al. [79] and 2.5 x 1.75 mm reservoir electrodes. The overlapping edge each transport electrode used a triangle pattern to create electrode interdigitation and promote droplet transport (Figure 5.13b). This design used only three reservoirs to allow for more DMF chips to be fabricated on one wafer. DI water was loaded onto the DMF chip using a variable micropipette prior to device encapsulation.

Initial attempts to manually perform droplet transport resulted in failure. Figure 5.14 depicts a failed attempt where the advancing edge of the fluid was able to move while the receding end remained stationary. Factors that could have contributed to this result are the excess fluid volume and dielectric breakdown/electrolysis.
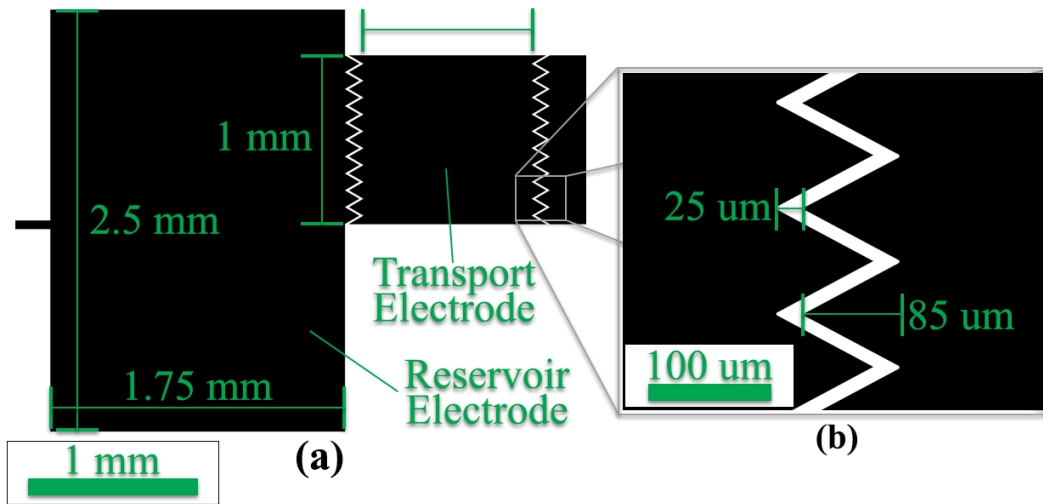
Figure 5.13: DMF device layout of prototype 1 showing (a) reservoir and transport electrode dimensions as well as (b) interdigitation dimensions

The excess DI water volume contributed to this result because the fluid was able to be deformed but not transported (Figure 5.14c-f). In this case, the radius of curvature of the DI water is large in the horizontal plane. This large radius of curvature results in a small surface tension force that maintains the circular shape of the fluid. With the addition of an electrowetting force, the fluid is unable to hold its shape and instead deforms. Possible solutions to this problem include the reduction of fluid volume or the increase of the channel gap. Increasing the channel gap distance was chosen because volumes under 1.5 uL were unable to be loaded reliably onto the DMF device prior to encapsulation.

Dielectric breakdown or electrolysis was also observed (Figure 5.14c-f). Dielectric breakdown or electrolysis is a critical failure mode for DMF devices because the device surface can be permanently modified. This surface modification would create random pinning points that cause droplets to stick during droplet transport or creation. Possible solutions to this problem include the use of a higher breakdown strength dielectric or increasing the dielectric thickness. Increasing the dielectric thickness was chosen to maintain a similar device fabrication process.
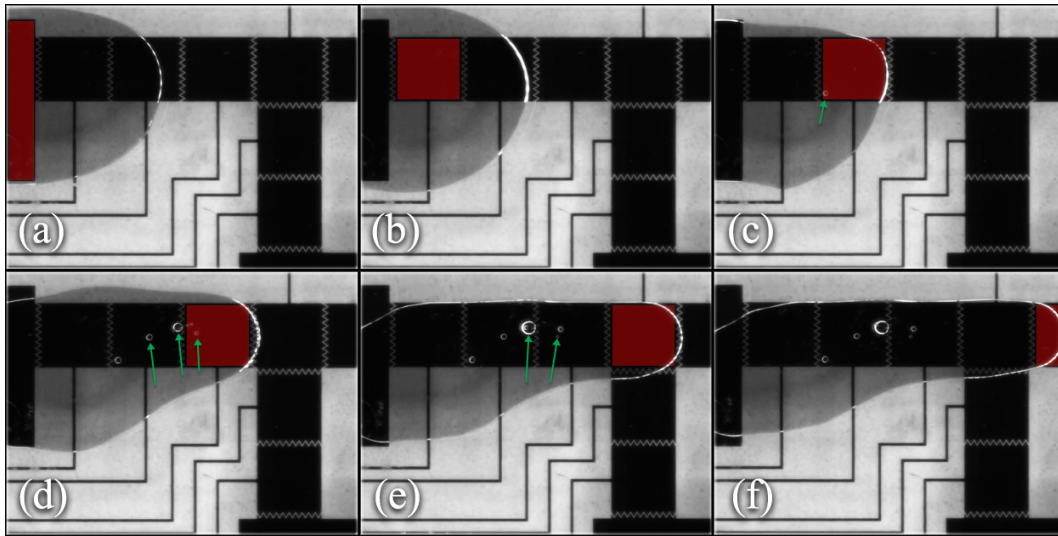
Figure 5.14: Image sequence from manual droplet transport attempt on DMF device prototype 1; Red electrodes are actuated while others are grounded; Green arrows in the images show observations of dielectric breakdown or electrolysis; This device was fabricated with the following specifications: 270 nm aluminum electrode layer, 360 nm silicon dioxide dielectric layer, and 60 um device channel gap; Testing was conducted using 1.5 uL of DI water on the custom NI control system with a 35 V_{RMS} 1kHz sinusoidal actuation signal

Successful droplet transport was demonstrated by moving a DI water test fluid from the reservoir, out three transport electrodes, back to the reservoir (Figure 5.15a-f). This result was achieved after the device channel gap was increased and the dielectric thickness was increased. The device channel gap was increased from 60 to 120 um through the use of an two additional strips of double-sided adhesive. The dielectric thickness was increased from 360 to 460 nm through the fabrication process. To further prevent dielectric breakdown/electrolysis, the necessary minimum actuation voltage was determined by ramping the signal incrementally until the electrowetting was observed. This strategy was used in all following test protocols. This manual droplet transport protocol was conducted numerous times to fulfill the goal of manual droplet transport.

Automated droplet transport was successfully demonstrated with the use of the custom National Instruments VI. The droplet was transported from one reservoir to another (Figure 5.16a-h). This automated droplet transport process was conducted numerous times without dielectric breakdown/electrolysis to fulfill the goal of automated droplet transport.
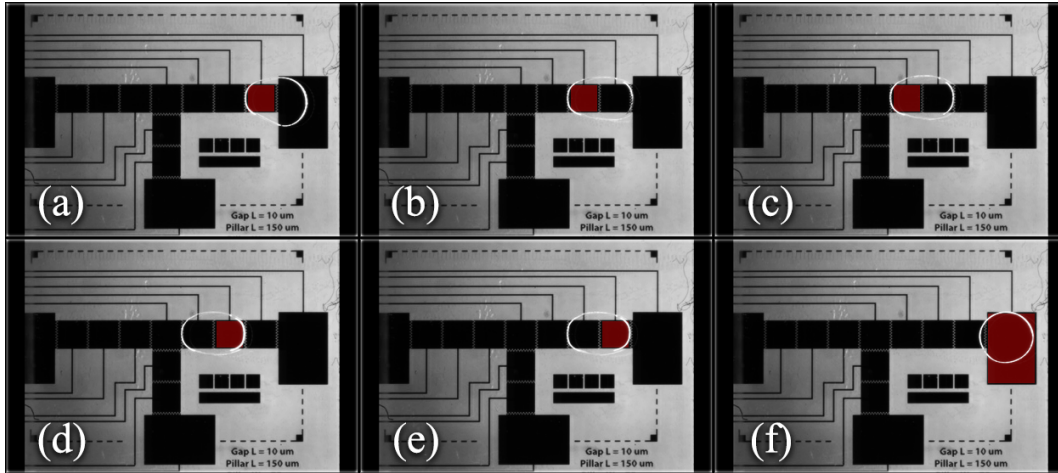
Figure 5.15: Image sequence from the second manual droplet transport attempt on DMF device prototype 1; Red electrodes are actuated while others are grounded; This device was fabricated with the following specifications: 216 nm aluminum electrode layer, 460 nm silicon dioxide dielectric layer, and 120 um device channel gap; Testing was conducted using 1.5 uL of DI water on the custom NI control system with a 35 V_{RMS} 1kHz sinusoidal actuation signal

Figure 5.16: Image sequence from an automated droplet transport attempt on DMF device prototype 1; Red electrodes are actuated while others are grounded; This device was fabricated with the following specifications: 216 nm aluminum electrode layer, 460 nm silicon dioxide dielectric layer, and 120 um device channel gap; Testing was conducted using 1.5 uL of DI water on the custom NI control system with a 35 V_{RMS} 1kHz sinusoidal actuation signal

5.1.2 Automated Droplet Creation

Automated creation of DI water droplets using resulted in partial success. In this protocol, the test fluid was transported two electrodes from the reservoir (Figure 5.17a-b). All three electrodes were actuated (Figure 5.17b) until the center electrode was grounded (Figure 5.17c) to create a droplet (Figure 5.17d). While this attempt resulted in successful creation, the droplet was unable to be subsequently transported (Figure 5.17e). Factors that contributed to this result are the inconsistent volume of the created droplet and the sensitivity of the transport electrode to droplet size. The modification of the reservoir and transport electrodes as well as the method of interdigitation was chosen as the solution to achieving reliable droplet creation and transport.
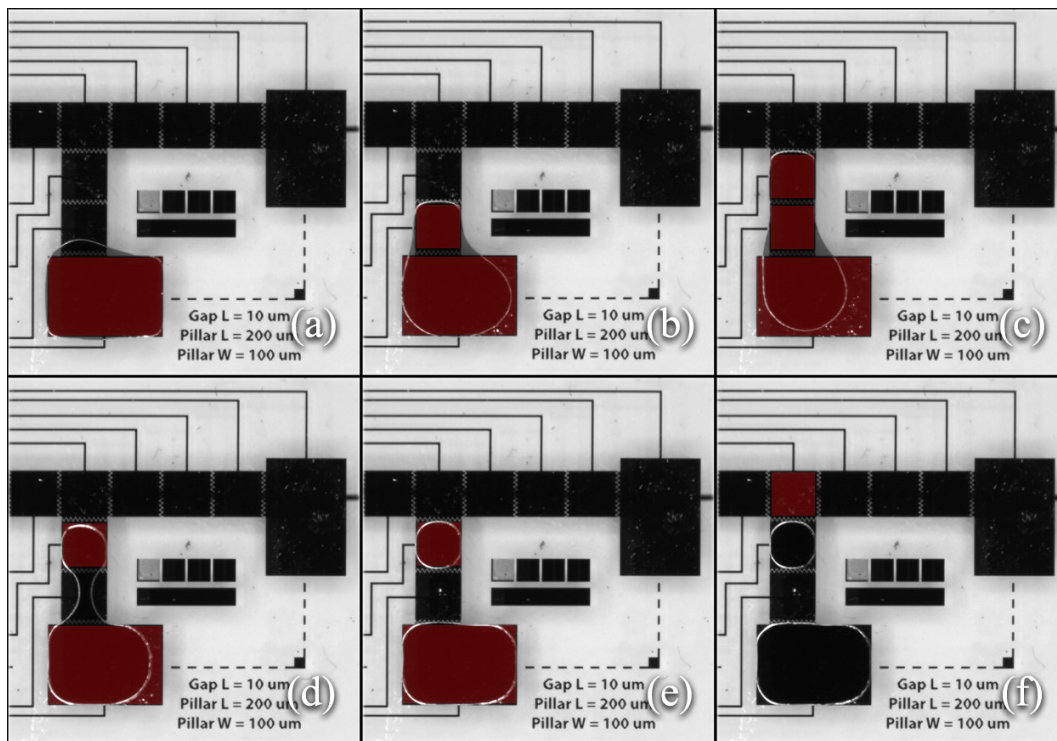
Figure 5.17: Images sequence from an automated droplet transport attempt on DMF device prototype 1; Red electrodes are actuated while others are grounded; This device was fabricated with the following specifications: 216 nm aluminum electrode layer, 460 nm silicon dioxide dielectric layer, and 120 um device channel gap; Testing was conducted using 1.5 uL of DI water on the custom NI control system with a 35.5 V_{RMS} 1kHz sinusoidal actuation signal

The demonstration of reliable automated droplet creation and transport was the next goal of DMF device prototyping. The second DMF device prototype seen in Figure 5.18 consisted of 1 x 1 mm transport electrodes based on the work of Cho et al. [83] as well as reservoir electrodes based on the work of Jagath et al. [107]. The transport electrode interdigitation design aimed to provide increase penetration electrodes in order to reduce the sensitivity to smaller volumes of droplets. The TC reservoir design aimed to target a consisting necking point to promote robust droplet creation. The C-reservoir electrode was used to deliver fluid while the T-cutting electrode was used to create a necking point closer to the center of the electrode. In addition, the creation electrode was designed to have a larger surface area than the transport electrodes.
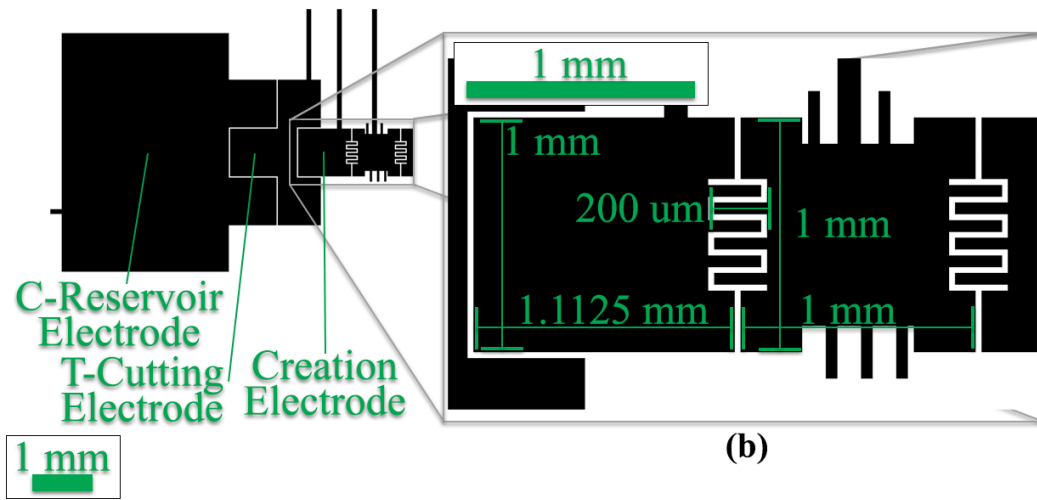
Figure 5.18: DMF device layout of prototype 2 showing (a) TC reservoir and transport electrode geometry as well as (b) key design dimensions

Initial attempts to demonstrate automated droplet creation, transport, and mixing on DMF prototype 2 resulted in partial success. While droplet creation and transport was successfully demonstrated from one reservoir, the evidence of dielectric breakdown or electrolysis was observed in the other (Figure 5.19e). This failure was likely due to local defects in the device surface. Works by Liu [66], Drygiannakis [70], and Papathanasiou [67] show evidence of breakdown that occurs before actuation voltages are reached in various materials. Future devices used a SU-8 3005 dielectric to prevent dielectric breakdown or electrolysis. SU-8 films are coated using spin coating and have a relative permittivity of 3.0. Future devices required actuation voltages of 140 and 162 V.

In addition, droplet creation was only able to be achieved by pulling the droplet past the creation electrode (Figure 5.19d). Droplet creation relies on the pressure difference created between the ends and center of the fluid. This pressure difference is created when the fluid is pressed between two surfaces and subsequently stretched by displacing the contact line at both ends. Cho et al. describes the dependence of the necessary pressure difference to induce necking on the channel gap distance and contact line displacement [83]. The gap distance was unable to be reduced because of the minimum volume able to be loaded onto the device. Future devices used a modified electrode geometry to promote reliable contact line displacement through droplet transport.
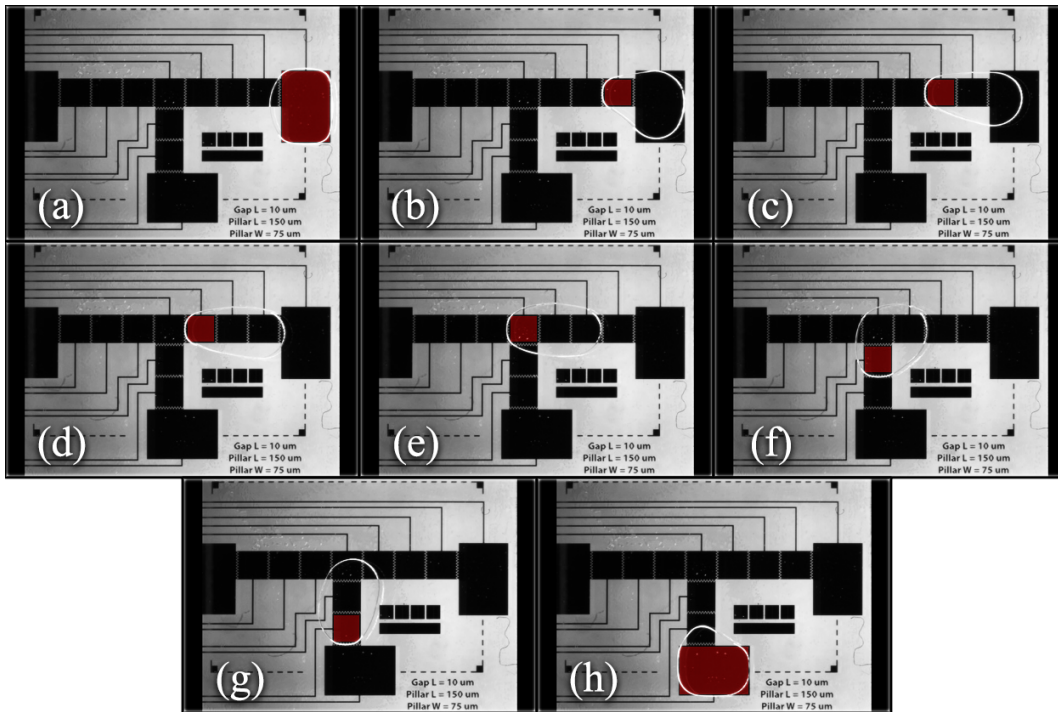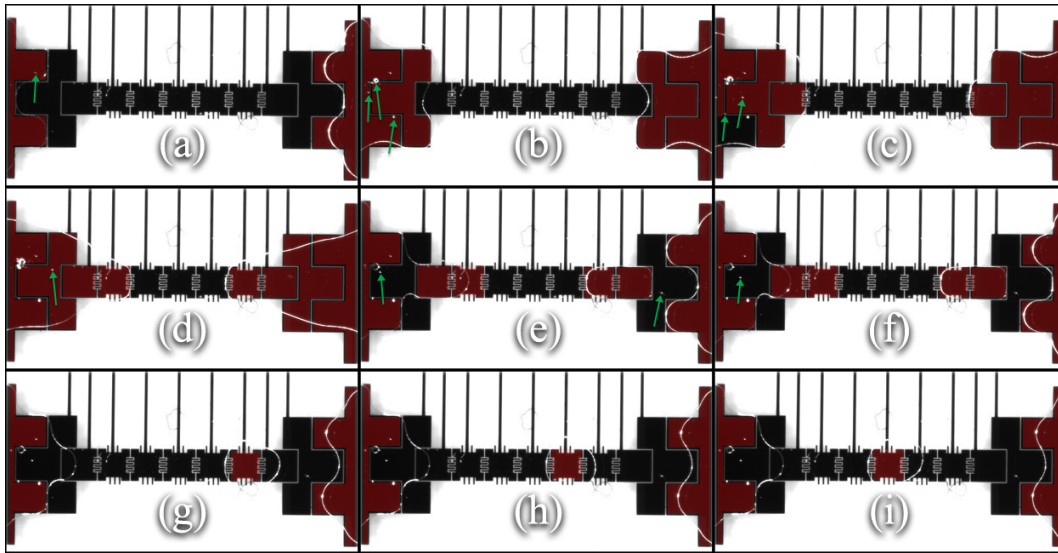
Figure 5.19: Image sequence from an automated droplet transport creation protocol on DMF device prototype 2; Red electrodes are actuated while others are grounded; Green arrows in the images show observations of dielectric breakdown or electrolysis; This device was fabricated with the following specifications: a 572 nm aluminum electrode layer, a 707 nm silicon dioxide dielectric layer, and a 120 um device channel gap; Testing was conducted with 1.5 uL of DI water at each reservoir using a 76 V_{RMS} 1kHz sinusoidal actuation signal.

5.1.3   Automated Droplet Creation, Transport, and Mixing

The demonstration of reliable automated droplet creation, transport and mixing was the final goal of DMF device prototyping. The final device prototype can be seen in Figure 5.20. This prototype was designed in an attempt to perform automated droplet transport and creation with both DI water and DNA laden fluids. The third DMF device prototype seen in the figure above was used to fabricate 6 devices with 1.5 x 1.5 mm transport electrodes based on the work of Jang et al. [80] along with revised reservoir electrodes based on the work of Jagath et al. [107]. The electrode interdigitation design aimed to increase the penetration contact area between electrodes. The reservoir electrode design used two C-reservoir electrodes in order to more increase the deliverable fluid volume while maintaining similar reliability. In addition, the creation electrode maintained a larger contact area than the transport electrode.
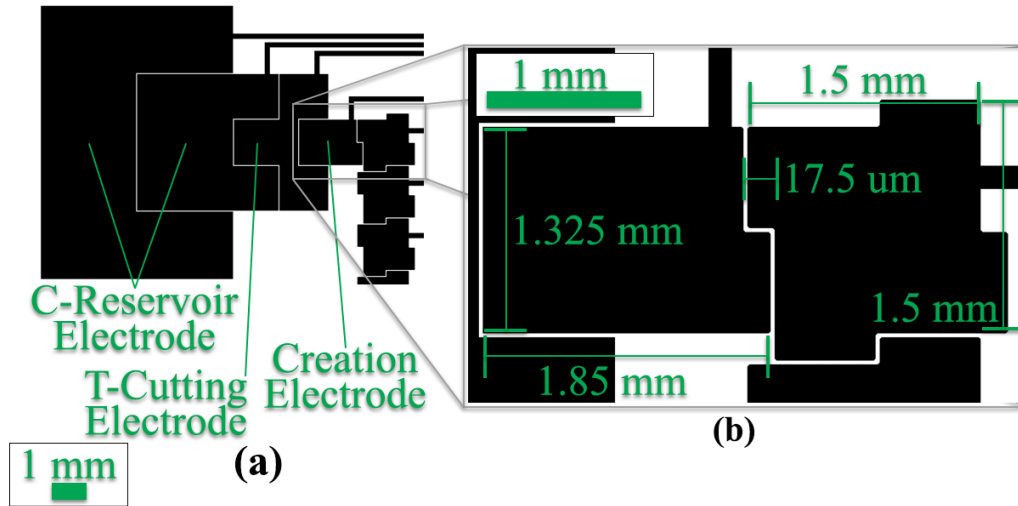
Figure 5.20: DMF device layout of prototype 3 showing (a) TCC reservoir and transport electrode geometry as well as (b) key design dimensions

Attempts to demonstrate automated droplet creation, transport, and mixing on DMF prototype 3 resulted in success. The automated protocol used in Figure 5.21 was able to create droplets simultaneously from both reservoirs (Figure 5.21a-f), transport both droplets to the center electrode (Figure 5.21g-j), and perform a mixing process (Figure 5.21k-n) without any breakdown or electrolysis. This DMF device design and protocol was able to fulfill the goal of automated droplet creation and transport. With this success, DMF prototype 3 was used with DNA laden fluid.
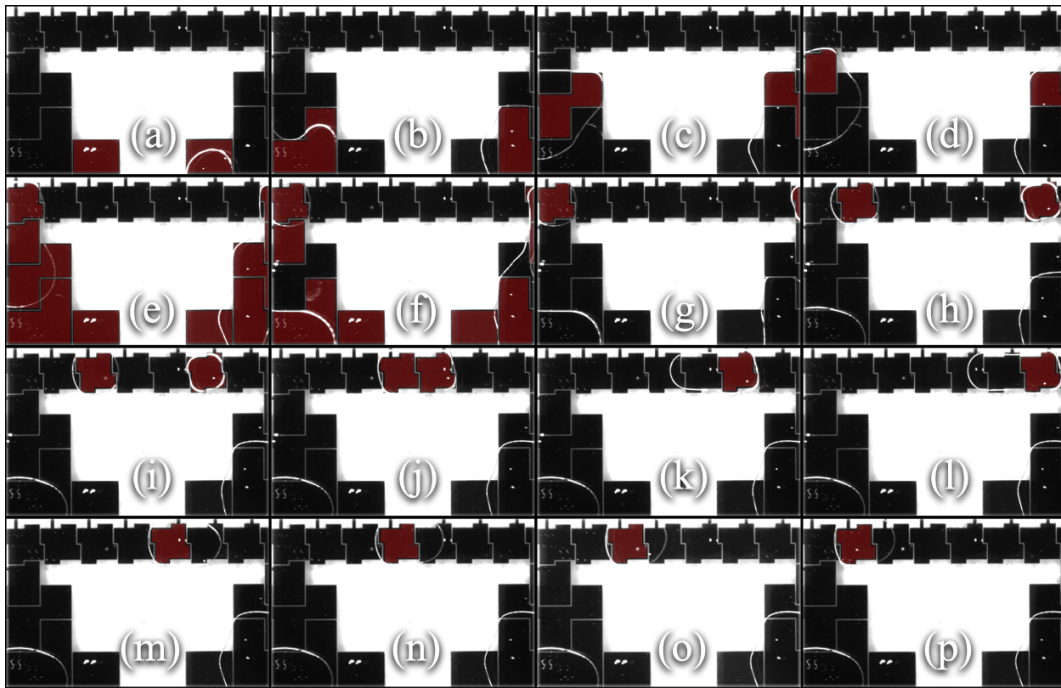
Figure 5.21: Image sequence from an automated droplet transport and creation protocol on DMF device prototype 3; Red electrodes are actuated while others are grounded; This device was fabricated with the following specifications: 443 nm aluminum electrode layer, 5.8 um SU-8 3005 dielectric layer, and 120 um device channel gap; Testing was conducted with 1.5 uL of DI water at each reservoir and DNA laden fluid using a 162 V_{RMS} 1kHz sinusoidal actuation signal

5.2   DNA Assembly

The second aim of this work was to demonstrate automated DNA assembly. This aim is subdivided into two aims: automated DNA assembly in (a) air-filled DMF device prototypes on the custom control system and (b) oil-filled DMF devices on the DropBot control system.

5.2.1   Air Medium: On Chip Mixing and Off Chip Incubation

The goal of this test was to examine the effects of DNA laden droplets in a device that manipulates droplets surrounded by air. The initial attempt to perform DNA assembly on DMF prototype 3 resulted in success. The automated protocol used in Figure 5.21 was performed using DNA laden droplets.

Droplets of DNA brick 1 and 2 solutions were first created and mixed together. The resultant product was extracted and incubated on a conventional chemical bench. Incubation was performed on a chemical bench because droplets seemed to be pinned to various areas of the device surface following the automated protocol. DNA gel electrophoresis was used to verify the success of automated droplet creation, transport, and mixing. Figure 5.22 depicts the imaged DNA gel used to verify the results of this DNA assembly process. As seen in the gel, each DNA brick is approximately 125 base pairs long while on-chip and on-bench protocols both resulted in lengths of 250 base pairs. With the validation of droplet creation, transport, and mixing with DNA laden droplets, the goal of automated DNA assembly in an air medium was fulfilled.
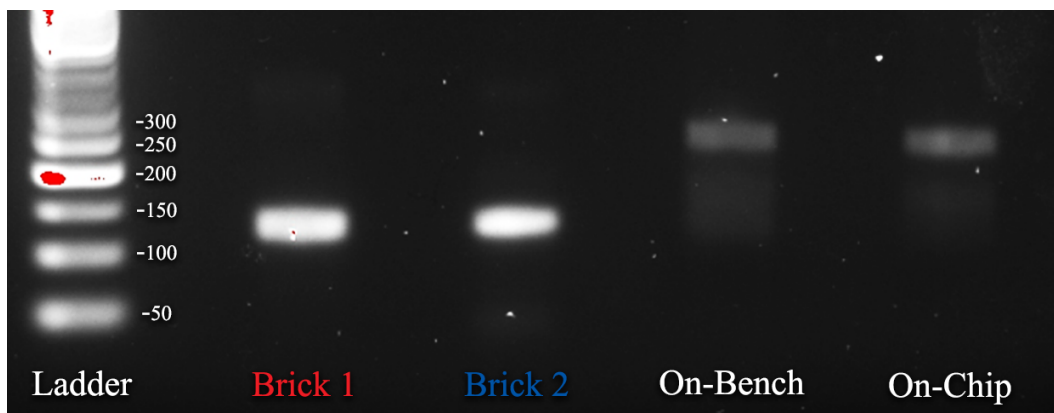
Figure 5.22: Imaged DNA electrophoresis gel comparing DNA Brick 1, DNA Brick 2, on-bench DNA assembly, and DNA assembly with on-chip mixing

An issue encountered during this protocol was the pinning of droplets to transport electrodes where DNA laden droplets were mixed. Due to this issue, this device was unable to run more than one automated protocol reliably with DNA laden droplets. This issue was likely caused by biofouling. Biofouling is the adsorption of biological molecules on surfaces. Adsorbed molecules have the potential to create random pinning points that could cause DMF device failure. Future DMF device used an oil medium to reduce the potential of biofouling from continuous DNA molecule and surface interactions [39, 99, 108–110]. An additional benefits of an oil medium is its ability to decrease droplet evaporation which is key during on chip incubation processes [39, 108].

While DNA assembly was demonstrated, the eventual goal of the DMF device is to be able to support the assembly of more than two DNA bricks. The DMF device must include more than two reservoirs to support additional reagents. Future devices will use a modified DMF device design and control system to support this goal.

5.2.2 Oil Medium: On Chip Mixing, Parking, and Off Chip Incubation

The demonstration of automated DNA assembly in an oil medium was the first goal of the final DMF device. The final DMF device design is depicted in Figure 5.23. This design consisted of two 4 x 17 contact pad arrays that are connected to the various elements using traces with widths of 30 um and 20 um separations. The location of the array from the edge of chip allowed for easy alignment of the device to the DropBot control system. The row of contact pads at the top and bottom of array were configured in order to enable the output of the actuation signal and also connect the device top-plate to ground. The large top and bottom electrodes were used as waste collection and outlet electrodes.
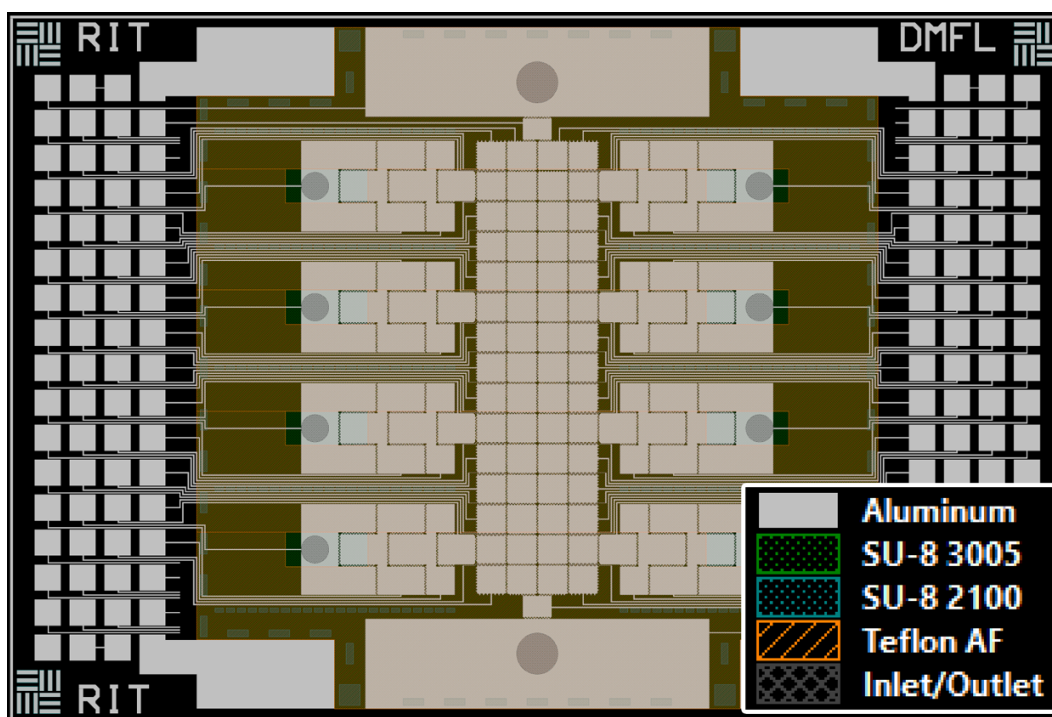
Figure 5.23: Full layout of final DMF chip; The inlet/outlet port locations are depicted for clarity

A close-up view of the reservoir and transport electrodes is depicted in Figure 5.24. The reservoir electrodes used a modified scheme of the TCC electrode design to support the larger density of metal traces necessary for a single layer process. The transport electrodes are based on the work of Fobel et al. [111] to maintain interdigitation between electrodes while supporting the density of metal traces necessary for a single layer process. This modification resulted in a reduced potential contact area between adjacent electrodes.

The modified DMF device structure to support the use of an oil medium is depicted in Figure 5.25. The placement of these port can be seen in Figure 5.24. Each port served as inlet/outlets to be used for reagent loading and extraction. Prior to testing, the DMF device was filled with silicone oil though the inlet/outlet ports using a variable micropipette.

Initial testing to demonstrate automated droplet creation on the final DMF device design with an oil medium resulted in success. The loading of DNA laden fluid into the DMF device is depicted in Figure 5.26a. This process is illustrated in Figure 5.25. In this process, a micropipette is used load fluid into the inlet while the reservoir electrodes were actuated. The loaded volumes of DNA brick 1 and 2 were subsequently used to create two droplets (Figure 5.26c-g).
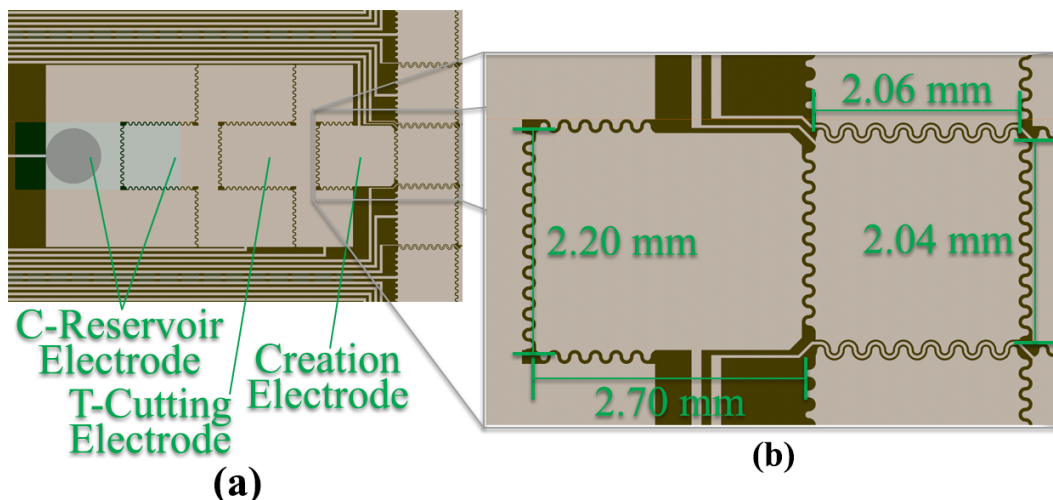
Figure 5.24: Final DMF device layout showing (a) TCC reservoir and transport electrode geometry as well as (b) key design dimensions
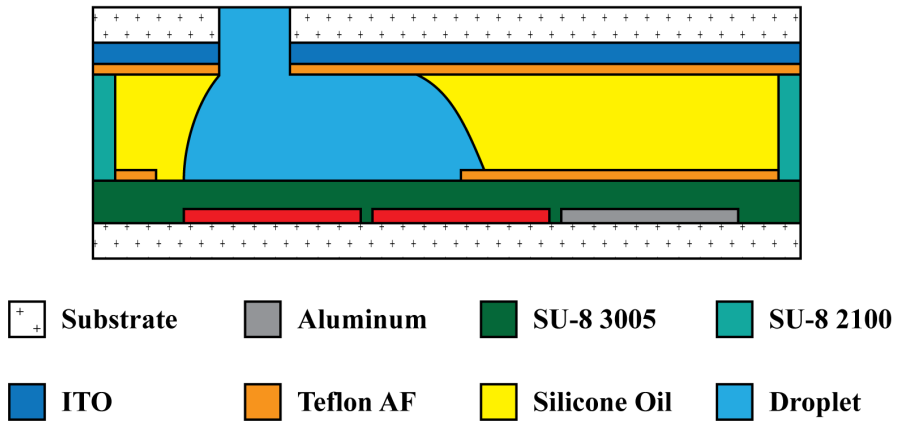
Figure 5.25: Schematic of final DMF device structure depicting the use of an oil medium as well as the method of fluid loading
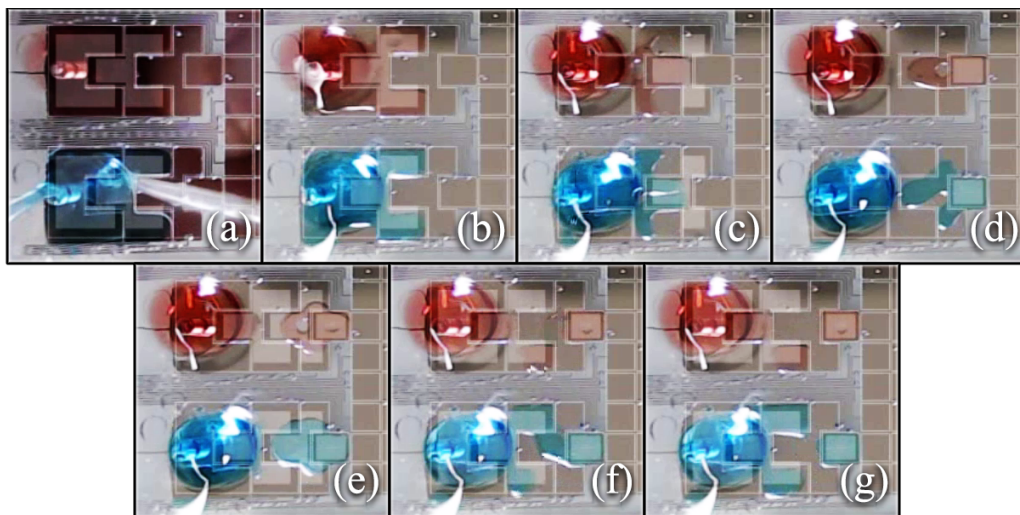
Figure 5.26: Image sequence from an automated droplet creation protocol using DNA brick 1 (red) and brick 2 (blue) on the final DMF device design; This device was fabricated using the following specifications: 100 nm aluminum electrode layer, 6.5 um SU-8 3005 dielectric layer, and 97 um SU-8 2100 negative photoresist device channel gap layer which also creates the channel gap and functions as a gasket template; Testing was conducted with DNA laden fluids using a 140 V_{RMS} 1kHz sinusoidal actuation signal; Fluid containing DNA brick 1 is dyed red while brick 2 is dyed blue and both solutions contained 0.1% of a mild Tween 20 surfactant

Initial testing to demonstrate automated droplet transport and mixing on the final DMF device design with an oil medium resulted in success. The automated transport and mixing of DNA bricks 1 and 2 is depicted in Figure 5.27. Each droplet was transported and subsequently merged onto one electrode. The merged droplets were then mixed for 10 minutes by performing droplet transport in a square pattern (Figure 5.27d). During this protocol, droplets seemed to be pinned continuously in one area (Figure 5.27i). This pinning is likely the attributed to the (i) droplet path during mixing, (ii) electrode number during mixing, (iii) surface defects/heterogeneity, (iv) biofouling, etc. When the receding edge of the fluid did not have enough time to catch up to the advancing edge droplet, droplet splitting occurred (Figure 5.27i). Works by Paik [112] and Fowler [113] suggest the use of multiple electrodes and a mixing pattern that includes the center electrode.
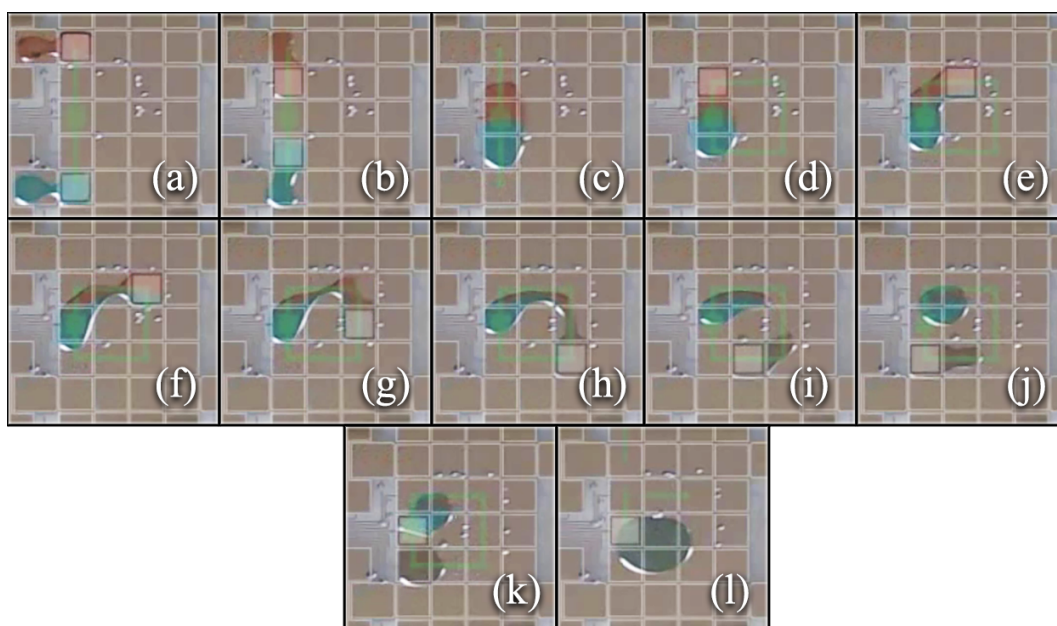
Figure 5.27: Image sequence from an automated droplet transport and mixing protocol using DNA brick 1 (red) and brick 2 (blue) on the final DMF device design; Red arrows in the images show observations of possible device failure modes

Mixed samples of mixed DNA bricks 1 and 2 were subsequently transported and extracted Figure 5.28. The mixed droplet was transported into a reservoir to be extracted. Droplets from a previous attempt was observed on the C-reservoir electrode (Figure 5.28a). Because of the low volume of this previous attempt, the sample was unable to be extracted at first. An additional protocol was performed while the first sample was parked on the C-reservoir electrode. With the added volume, the sample was able to be extracted.

After extracting the mixed DNA solutions, samples were incubated on a chemical bench for 10 minutes at 70 °C and placed into DNA gels for electrophoresis and imaging. The results of each protocol were examined by analyzing the DNA gels in order to verify the success of the assembly protocols. Figure 5.29 depicts results from the protocols performed on the final DMF device design where DMF1 denoted the sample from normal on-chip mixing process while DMF2 denoted the sample from the addition of droplet parking. As seen in the DNA gel, each DNA brick resulted approximately 125 base pairs, on-bench protocol resulted in 250 base pairs, and both DMF protocols resulted in 250 base pairs.

Figure 5.28: Image sequence from an automated droplet transport and extraction protocol using DNA brick 1 (red) and brick 2 (blue) on the final DMF device design
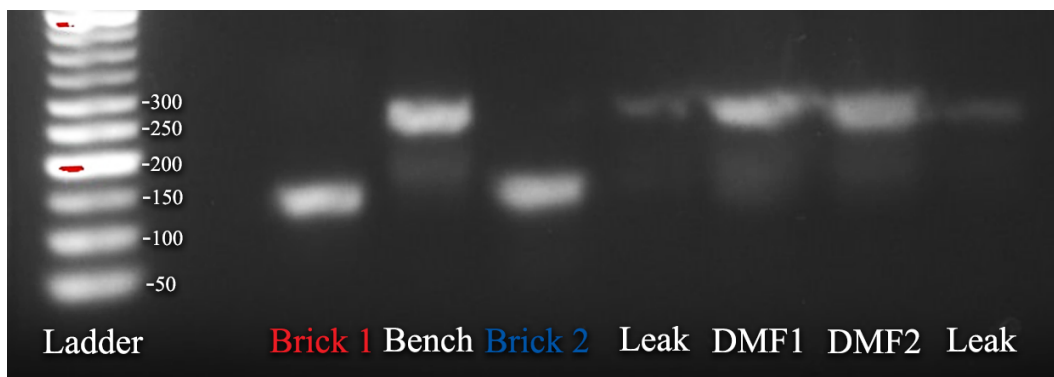
Figure 5.29: Imaged DNA electrophoresis gel comparing DNA Brick 1, DNA Brick 2, on-bench DNA assembly, DNA assembly with on-chip mixing (DMF1), and DNA assembly with on-chip mixing and parking (DMF2)

5.2.3 Oil Medium: On Chip Mixing, Parking, and Incubation

The demonstration of on chip incubation was the goal of this additional testing using the final DMF device. Further testing to demonstrate DNA assembly with on chip incubation resulted in success. The automated creation of two droplets using loaded volumes of DNA brick 1 and 2 is depicted in Figure 5.30. In comparison to previous tests, this protocol showed no evidence of air voids or oil shells that propagate.
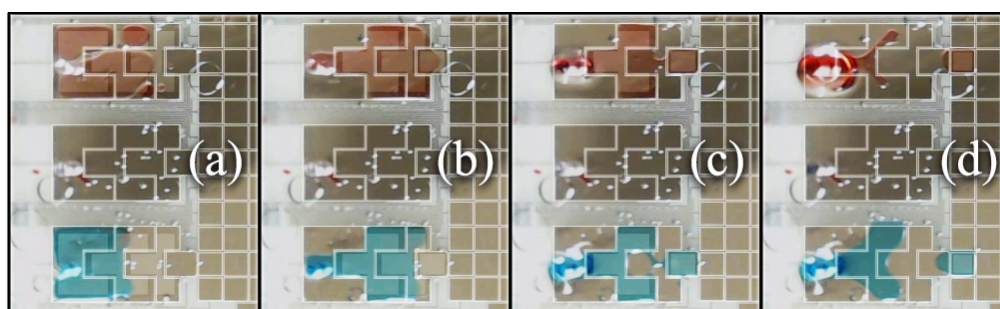
Figure 5.30: Image sequence from the second automated droplet creation protocol using DNA brick 1 (red) and brick 2 (blue) on the final DMF device design; This device was fabricated using the following specifications: 100 nm aluminum electrode layer, 6.5 um SU-8 3005 dielectric layer, and 97 um SU-8 2100 negative photoresist device channel gap layer which also creates the channel gap and functions as a gasket template; Testing was conducted with DNA laden fluids using a 140 V_{RMS} 1kHz sinusoidal actuation signal; Fluid containing DNA brick 1 is dyed red while brick 2 is dyed blue and both solutions contained 0.1% of a mild Tween 20 surfactant

Testing to demonstrate automated droplet transport and mixing on the final DMF device design with an oil medium resulted in success. The automated droplet mixing process is depicted during the beginning (Figure 5.31a-g) and end (Figure 5.31h-n) of the 30 minute room temperature initial incubation. Compared to Figure 5.27, this protocol used a series of two electrodes to transport the electrode in a square pattern.

Testing to demonstrate on chip incubation with the final DMF device design in an oil medium resulted in success. The automated on-chip incubation process is depicted in Figure 5.32. The mixed droplet was first parked on a single electrode (Figure 5.32a). A resistive foil heater was then set to 70 °C to perform the on-chip incubation for 60 minutes (Figure 5.32b).
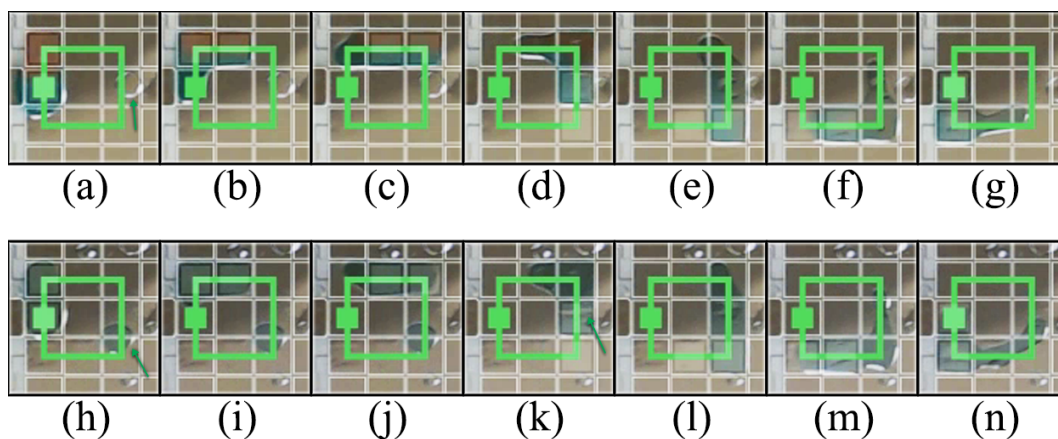
Figure 5.31: Image sequence from the second automated droplet transport and mixing protocol using DNA brick 1 (red) and brick 2 (blue) on the final DMF device design
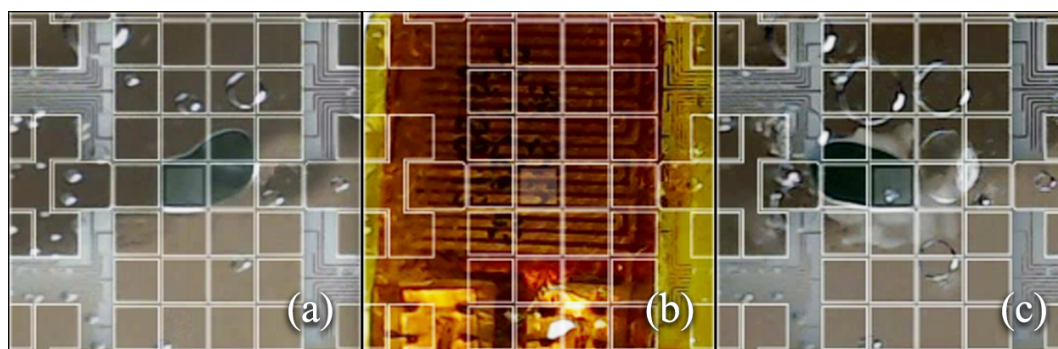
Figure 5.32: Image sequence from the parking and incubation protocol using DNA brick 1 (red) and brick 2 (blue) on the final DMF device design

Testing to demonstrate automated droplet transport and extraction of on the final DMF device design with an oil medium resulted in success. The automated droplet transport and extraction of mixed and incubated DNA brick 1 and 2 samples is depicted in Figure 5.33. From the high temperature incubation, reagents of DNA brick 1 from a previous protocol were observed in the oulet reservoir (Figure 5.33a). In order to extract the sample an additional volume of DI water was injected into the reservoir (Figure 5.33g).

DNA gel electrophoresis results confirmed the successful demonstration of on chip mixing and incubation DNA assembly process on the final DMF device design. The results from automated protocols performed on the final DMF device design with on-chip incubation is depicted in Figure 5.34. As seen in the DNA gel, each DNA brick resulted 125 base pairs while on-bench and on DMF resulted in 250 base pairs. The lower intensity of imaged samples from the DMF device can be explained by the injected additional volume of DI water used to extract the sample. DNA assembly on the DMF device was able to produce a product with a similar number of base pairs to the on-bench protocol. Through the course of this protocol, the successful demonstration of DNA assembly with on chip incubation was fulfilled.
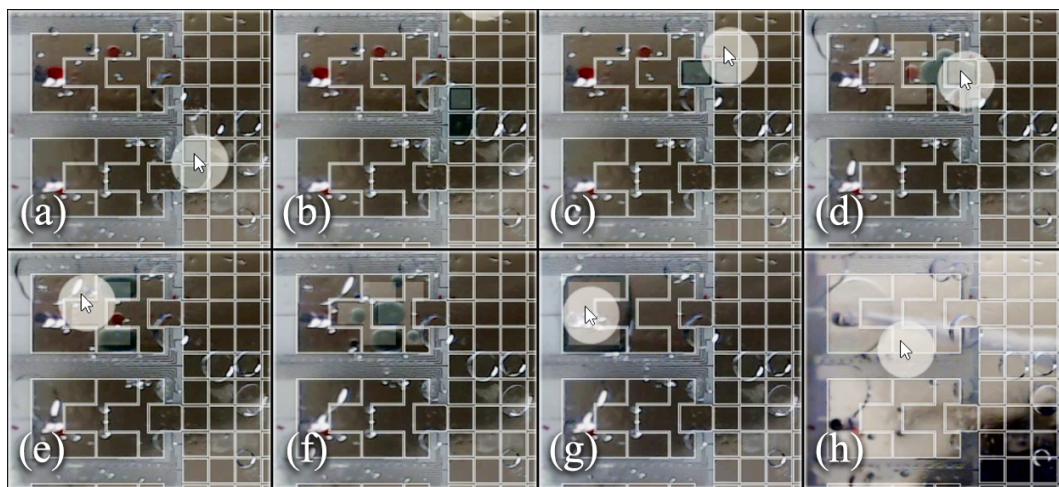
Figure 5.33: Image sequence from the second automated droplet transport and extraction protocol using DNA brick 1 (red) and brick 2 (blue) on the final DMF device design
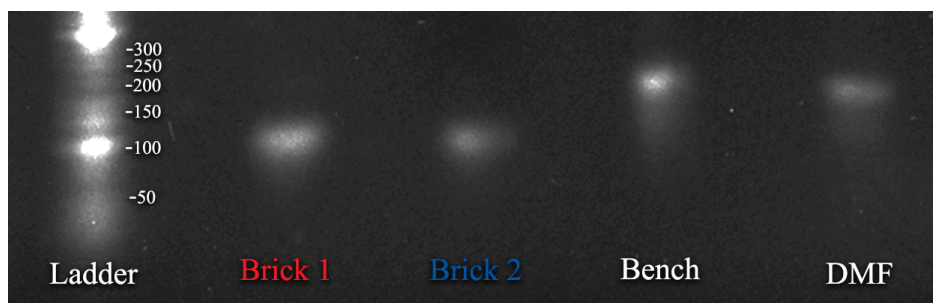
Figure 5.34: Image sequence from the second automated droplet transport and mixing protocol using DNA brick 1 (red) and brick 2 (blue) on the final DMF device design

6 Conclusion

6.1 Summary of Thesis Work

This investigation sought to demonstrate the applicability of DNA assembly on a DMF device. To achieve this goal, an iterative prototyping strategy was used. This process involved the design of an electrode layout, the fabrication of the device, and the testing of crucial fluid handling functions until adequate performance was demonstrated using DI water. Devices were fabricated using standard microfabrication tools and techniques. Prototype testing was conducted through the use of a custom LabVIEW virtual instrument while final device design testing was conducted on the Sci-Bots DropBot platform. DNA assembly was performed on DMF devices through the creation of two discrete droplets containing DNA Brick 1 and 2 with subsequent transport, mixing, and incubation steps to create the targeted DNA product. Results were validated through the use of a DNA gel to compare on-chip to on-bench assembly processes.

Through the prototyping process, important design considerations for a DMF device structure were determined. To prevent critical failures such as dielectric breakdown or electrolysis, a relatively thick SU-8 3005 negative photoresist is used as a dielectric layer. While it would increase the required actuation voltage, this design choice reduces the sensitivity of the device the variances in thickness and film quality. To enable droplet creation, the gap distance between the DMF chip and top plate is created and minimized through the use of a thick SU-8 2100 negative photoresist as a spacer layer. Using conventional microfabrication techniques allowed for the precise control and minimization of the device gap distance.

In addition to the DMF device structure, the device layout and electrode geometry was a crucial consideration for reliable DMF operation. During the prototyping process, the reservoir and transport electrode geometry was iterated until adequate performance was observed through DI water testing. The final reservoir geometry featured a TCC design. The C electrodes targeted predictable fluid delivery while the T electrode enabled the predictable of droplet cutting. The final transport electrode geometry featured a pinwheel design. This design targeted the use of a geometry with lower electrode surface area with higher interdigitation contact area. The final DMF device design featured a modified TCC reservoir and transport electrode geometry to ensure the connection of all actuation electrodes to pin pads using a one metal layer fabrication process.

Initial testing performed automated manipulations using DNA laden droplets in an air medium. DNA bricks were mixed on-chip and incubated on a chemical wet bench. After observing evidence of surface fouling during this initial testing process, the final DMF device design was supplemented with the use of a silicone oil medium. This was achieved by permanently bonding the DMF chip with the top plate with epoxy. The top plate included bored inlet/outlet ports and used the spacer layer as a gasket template. Followed testing included the use of the oil medium with on-bench and on-chip incubations. The success of DNA assembly was analyzed through the use of electrophoretic gel imaging. DMF device and bench top protocols yielded similar results with targeted base pair lengths of the assembly process to validate the demonstration of DNA assembly on a DMF device. Through this work, a DMF device was designed, fabricated, and to successfully fulfill the goal of automated DNA assembly. A summary of the design choices, protocol details, and observations of each iteration can be seen in Table 2. The successful results achieved in this work was published in a conference paper [114].

Table 2: Summary of device design iterations and observations

DMF Design	Prototype 1	Prototype 2	Prototype 3	Final Device
Reservoir Geometry	Schertzer et al.	Jagath et al.	Jagath et al.	Jagath et al.
Interdigitation Geometry	Triangle Pattern	Cho et al.	Jang et al.	Sinusoidal Pattern
Dielectric Material	Silicon dioxide	Silicon dioxide	SU-8 3005	SU-8 3005
Channel Gap Material	Double-sided adhesive	Double-sided adhesive	SU-8 2100	SU-8 2100
Medium	Air	Air	Air	Oil
Test Fluid	DI water	DI water	DI water and DNA solutions	DI water and DNA solutions
Control System	Custom NI control system	Custom NI control system	Custom NI control system	Sci-Bots DropBot system
Advantages	Repeatable automated transport of large droplet	Repeatable automated transport of created droplet	Repeatable droplet creation, transport, mixing	Repeatable droplet creation, transport, mixing and DNA assembly with on and off chip incubation
Disadvantages	Unreliable transport of created droplet and breakdown	Unreliable droplet creation and breakdown	Biofouling and high actuation voltage	Random pinning points after extended protocols
Proposed Changes	Increased channel gap distance and dielectric thickness	New dielectric material and modified electrode geometries	New device design to support oil medium and additional reagents	Characterization of random pinning points and device stress testing

6.2 Future Work

While this work was able to successfully demonstrate DNA assembly on a DMF device, much work is still necessary to create a complete LoC platform able to reliably demonstrate an automated full DNA synthesis process. Possible future work include: the integration of an on-chip resistive heater and sensor for droplet incubation, device stress testing and failure analysis, optimization of device layout and fabrication, and the integration of oligonucleotide synthesis.

Through the device testing, various failure modes were observed: dielectric breakdown, electrolysis, and biofouling as seen in Figure 6.35. Though these issues did not prevent the demonstration of DNA assembly, droplet interactions with random pinning points commonly caused unpredictable droplet creation and transport. At times, small satellite droplets were created from the droplet pinning. For a lengthy protocol that performs many assembly processes, this issue could be a large failure mode for accurate synthesis. To ensure device would be a suitable platform for the synthesis of long sequences of DNA, it is critical to quantify and mitigate the effects of random pinning points from dielectric breakdown, electrolysis, and biofouling.

Figure 6.35: Image sequence from the second automated droplet transport and extraction protocol where a droplet is spontaneously created from a random pinning point on the device surface

The effects of random pinning points must be solved by the determination of exact cause of the problem. This can be done in a number of steps. First, the surface quality at each layer can be examined through surface roughness measurements or scanning electron microscopy with energy-dispersive X-ray spectroscopy. By performing this analysis the possibility of fabrication induced failures can be examined. Secondly, electrical stress testing could provide insight into the robustness of future device dielectrics. Performing these tests with various dielectric materials would allow for the determination of an optimal dielectric material. Lastly, testing to characterize the severity of biofouling would ensure it can be mitigated. These tests can be done on simpler devices using the same materials.

The integration of an on-chip resistive heater and sensor are key to creating a complete LoC platform for DNA synthesis. During the course of this work, an external resistive foil heater was used to perform the incubation processes. Because the DropBot system was unable to support alternative placements of this heater, the view of the incubation process was obscured. By integrating this heater and sensor on-chip, higher control of the incubation process can be achieved. With the need to integrate a separate control system for incubation automation, this heater may better suited for integration in the control system.

The ultimate goal that motivated this thesis work is the integration of the entire DNA synthesis process. To do so, enzymatic oligonucleotide synthesis must be demonstrated. Oligonucleotide synthesis processes use solid support materials to attach nucleotide carrying samples. In order to ensure synthesis accuracy, solid supports are immobilized to perform necessary washing cycles to remove synthesis reagents from the solution. Though conventional microarray platform substrates act as the solid support materials, microfluidic solutions often use polystyrene beads to attach nucleotides carrying samples. To support this application, it is necessary to involve a form of filtration to immobilize solid supports while allowing the necessary washing cycles. While mechanical filtration has been used before, an emerging solution is the use of magnetic filtration. Using a magnetic field, polystyrene beads are immobilized while electrowetting on dielectric performs the washing cycles. Integration of this protocol may be best suited for the control system.

References

[1] S. Ma, N. Tang, and J. Tian, "DNA Synthesis, Assembly and Applications in Synthetic Biology," *Current opinion in chemical biology*, vol. 16, no. 3-4, pp. 260–267, Aug. 2012. [Online]. Available: https://www.ncbi.nlm.nih.gov/pmc/articles/PMC3424320/

[2] S. Kosuri and G. M. Church, "Large-scale de novo DNA synthesis: technologies and applications," *Nature Methods*, vol. 11, no. 5, pp. 499–507, May 2014, number: 5 Publisher: Nature Publishing Group. [Online]. Available: https://www.nature.com/articles/nmeth.2918

[3] S. Palluk, D. H. Arlow, T. de Rond, S. Barthel, J. S. Kang, R. Bector, H. M. Baghdassarian, A. N. Truong, P. W. Kim, A. K. Singh, N. J. Hillson, and J. D. Keasling, "De novo DNA synthesis using polymerase-nucleotide conjugates," *Nature Biotechnology*, vol. 36, no. 7, pp. 645–650, Aug. 2018, number: 7 Publisher: Nature Publishing Group. [Online]. Available: https://www.nature.com/articles/nbt.4173

[4] M. A. Jensen and R. W. Davis, "Template-Independent Enzymatic Oligonucleotide Synthesis (TiEOS): Its History, Prospects, and Challenges," *Biochemistry*, vol. 57, no. 12, pp. 1821–1832, Mar. 2018, publisher: American Chemical Society. [Online]. Available: https://doi.org/10.1021/acs.biochem.7b00937

[5] H. H. Lee, R. Kalhor, N. Goela, J. Bolot, and G. M. Church, "Terminator-free template-independent enzymatic DNA synthesis for digital information storage," *Nature Communications*, vol. 10, no. 1, p. 2383, Jun. 2019, number: 1 Publisher: Nature Publishing Group. [Online]. Available: http://www.nature.com/articles/s41467-019-10258-1

[6] T. Taniguchi, T. Torii, and T. Higuchi, "Chemical reactions in microdroplets by electrostatic manipulation of droplets in liquid media," *Lab on a Chip*, vol. 2, no. 1, pp. 19–23, 2002, publisher: Royal Society of Chemistry. [Online]. Available: http://pubs.rsc.org/en/content/articlelanding/2002/lc/b108739h

[7] D. Chatterjee, B. Hetayothin, A. R. Wheeler, D. J. King, and R. L. Garrell, "Droplet-based microfluidics with nonaqueous solvents and solutions," *Lab on a Chip*, vol. 6, no. 2, pp. 199–206, Jan. 2006, publisher: The Royal Society of Chemistry. [Online]. Available: http://pubs.rsc.org/en/content/articlelanding/2006/lc/b515566e

[8] R. B. Fair, A. Khlystov, T. D. Tailor, V. Ivanov, R. D. Evans, V. Srinivasan, V. K. Pamula, M. G. Pollack, P. B. Griffin, and J. Zhou, "Chemical and Biological Applications of Digital-Microfluidic Devices," *IEEE Design Test of Computers*, vol. 24, no. 1, pp. 10–24, Jan. 2007, conference Name: IEEE Design Test of Computers.

[9] M. J. Jebrail, M. S. Bartsch, and K. D. Patel, "Digital microfluidics: a versatile tool for applications in chemistry, biology and medicine," *Lab on a Chip*, vol. 12, no. 14, pp. 2452–2463, Jun. 2012, publisher: The Royal Society of Chemistry. [Online]. Available: http://pubs.rsc.org/en/content/articlelanding/2012/lc/c2lc40318h

[10] K. Choi, A. H. Ng, R. Fobel, and A. R. Wheeler, "Digital Microfluidics," *Annual Review of Analytical Chemistry*, vol. 5, no. 1, pp. 413–440, 2012, _-eprint: https://doi.org/10.1146/annurev-anchem-062011-143028. [Online]. Available: https://doi.org/10.1146/annurev-anchem-062011-143028

[11] V. Rastogi and O. D. Velev, "Development and evaluation of realistic microbioassays in freely suspended droplets on a chip," *Biomicrofluidics*, vol. 1, no. 1, p. 014107, Mar. 2007, publisher: American Institute of Physics. [Online]. Available: https://aip.scitation.org/doi/abs/10.1063/1.2714185

[12] M. J. Jebrail and A. R. Wheeler, "Let's get digital: digitizing chemical biology with microfluidics," *Current Opinion in Chemical Biology*, vol. 14, no. 5, pp. 574–581, Oct. 2010. [Online]. Available: http://www.sciencedirect.com/science/article/pii/S1367593110000955

[13] N. Vergauwe, D. Witters, F. Ceyssens, S. Vermeir, B. Verbruggen, R. Puers, and J. Lammertyn, "A versatile electrowetting-based digital microfluidic platform for quantitative homogeneous and heterogeneous bio-assays," *Journal of Micromechanics and Microengineering*, vol. 21, no. 5, p. 054026, Apr. 2011, publisher: IOP Publishing. [Online]. Available: https://doi.org/10.1088/0960-1317/21/5/054026

[14] A. H. Ng, B. B. Li, M. D. Chamberlain, and A. R. Wheeler, "Digital Microfluidic Cell Culture," *Annual Review of Biomedical Engineering*, vol. 17, no. 1, pp. 91–112, 2015, _eprint: https://doi.org/10.1146/annurev-bioeng-071114-040808. [Online]. Available: https://doi.org/10.1146/annurev-bioeng-071114-040808

[15] E. Wulff-Burchfield, W. A. Schell, A. E. Eckhardt, M. G. Pollack, Z. Hua, J. L. Rouse, V. K. Pamula, V. Srinivasan, J. L. Benton, B. D. Alexander, D. A. Wilfret, M. Kraft, C. B. Cairns, J. R. Perfect, and T. G. Mitchell, "Microfluidic platform versus conventional real-time polymerase chain reaction for the detection of Mycoplasma pneumoniae in respiratory specimens," *Diagnostic Microbiology and Infectious Disease*, vol. 67, no. 1, pp. 22–29, May 2010. [Online]. Available: https://www.sciencedirect.com/science/article/pii/S0732889309005112

[16] R. S. Sista, A. E. Eckhardt, T. Wang, C. Graham, J. L. Rouse, S. M. Norton, V. Srinivasan, M. G. Pollack, A. A. Tolun, D. Bali, D. S. Millington, and V. K. Pamula, "Digital Microfluidic Platform for Multiplexing Enzyme Assays: Implications for Lysosomal Storage Disease Screening in Newborns," *Clinical Chemistry*, vol. 57, no. 10, pp. 1444–1451, Oct. 2011. [Online]. Available: https://doi.org/10.1373/clinchem.2011.163139

[17] M. J.ăJebrail, H. Yang, J. M.ăMudrik, N. M.ăLafrenière, C. McRoberts, O. Y.ăAl-Dirbashi, L. Fisher, P. Chakraborty, and A. R.ăWheeler, "A digital microfluidic method for dried blood spot analysis," *Lab on a Chip*, vol. 11, no. 19, pp. 3218–3224, 2011, publisher: Royal Society of Chemistry. [Online]. Available: http://pubs.rsc.org/en/content/articlelanding/2011/lc/c1lc20524b

[18] M. G. Pollack, V. K. Pamula, V. Srinivasan, and A. E. Eckhardt, "Applications of electrowetting-based digital microfluidics in clinical diagnostics," *Expert Review of Molecular Diagnostics*, vol. 11, no. 4, pp. 393–407, May 2011, publisher: Taylor & Francis _eprint: https://doi.org/10.1586/erm.11.22. [Online]. Available: https://doi.org/10.1586/erm.11.22

[19] E. Samiei, M. Tabrizian, and M. Hoorfar, "A review of digital microfluidics as portable platforms for lab-on a-chip applications," *Lab on a Chip*, vol. 16, no. 13, pp. 2376–2396, 2016, publisher: Royal Society of Chemistry. [Online]. Available: http://pubs.rsc.org/en/content/articlelanding/2016/lc/c6lc00387g

[20] H. Moon, S. K. Cho, R. L. Garrell, and C.-J. . Kim, "Low voltage electrowetting-on-dielectric," *Journal of Applied Physics*, vol. 92, no. 7, pp. 4080–4087, Sep. 2002, publisher: American Institute of Physics. [Online]. Available: http://aip.scitation.org/doi/abs/10.1063/1.1504171

[21] J. Lee, H. Moon, J. Fowler, T. Schoellhammer, and C.-J. Kim, "Electrowetting and electrowetting-on-dielectric for microscale liquid handling," *Sensors and Actuators A: Physical*, vol. 95, no. 2, pp. 259–268, Jan. 2002. [Online]. Available: http://www.sciencedirect.com/science/article/pii/S0924424701007348

[22] W. C. Nelson and C.-J. . Kim, "Droplet Actuation by Electrowetting-on-Dielectric (EWOD): A Review," *Journal of Adhesion Science and Technology*, vol. 26, no. 12-17, pp. 1747–1771, Sep. 2012, publisher: Taylor & Francis _eprint: https://www.tandfonline.com/doi/pdf/10.1163/156856111X599562. [Online]. Available: https://www.tandfonline.com/doi/abs/10.1163/156856111X599562

[23] M. Abdelgawad and A. R. Wheeler, "The Digital Revolution: A New Paradigm for Microfluidics," *Advanced Materials*, vol. 21, no. 8, pp. 920–925, 2009, _eprint: https://onlinelibrary.wiley.com/doi/pdf/10.1002/adma.200802244. [Online]. Available: https://onlinelibrary.wiley.com/doi/abs/10.1002/adma.200802244

[24] D. G. Gibson, "Synthesis of DNA fragments in yeast by one-step assembly of overlapping oligonucleotides," *Nucleic Acids Research*, vol. 37, no. 20, pp. 6984–6990, Nov. 2009, publisher: Oxford Academic. [Online]. Available: https://academic.oup.com/nar/article/37/20/6984/1105736

[25] T. Ellis, T. Adie, and G. S. Baldwin, "DNA assembly for synthetic biology: from parts to pathways and beyond," *Integrative Biology*, vol. 3, no. 2, pp. 109–118, Feb. 2011. [Online]. Available: https://doi.org/10.1039/c0ib00070a

[26] H. W. Matthes, W. M. Zenke, T. Grundström, A. Staub, M. Wintzerith, and P. Chambon, "Simultaneous rapid chemical synthesis of over one hundred oligonucleotides on a microscale," *The EMBO Journal*, vol. 3, no. 4, pp. 801–805, Apr. 1984, publisher: John Wiley & Sons, Ltd. [Online]. Available: http://www.embopress.org/doi/abs/10.1002/j.1460-2075.1984.tb01888.x

[27] M. H. Caruthers, A. D. Barone, S. L. Beaucage, D. R. Dodds, E. F. Fisher, L. J. McBride, M. Matteucci, Z. Stabinsky, and J. Y. Tang, "[15] Chemical synthesis of deoxyoligonucleotides by the phosphoramidite method," in *Methods in Enzymology*, ser. Recombinant DNA Part E.   Academic Press, Jan. 1987, vol. 154, pp. 287–313. [Online]. Available: http://www.sciencedirect.com/science/article/pii/0076687987540812

[28] H. A. White, "Manual Oligonucleotide Synthesis Using the Phosphoramidite Method," in *New Nucleic Acid Techniques*, ser. Methods in Molecular Biology, J. M. Walker, Ed.   Totowa, NJ: Humana Press, 1988, pp. 193–213. [Online]. Available: https://doi.org/10.1385/0-89603-127-6:193

[29] B. H. Dahl, J. Nielsen, and O. Dahl, "Mechanistic studies on the phosphoramidite coupling reaction in oligonucleotide synthesis. I. Evidence for nudeophilic catalysis by tetrazole and rate variations with the phosphorus substituents," *Nucleic Acids Research*, vol. 15, no. 4, pp. 1729–1743, Feb. 1987. [Online]. Available: https://doi.org/10.1093/nar/15.4.1729

[30] N. Sinha, J. Biernat, J. McManus, and H. Köster, "Polymer support oligonucleotide synthesis XVIII1.2): use of -cyanoethyi-N,N-dialkylamino-/N-morpholino phosphoramidite of deoxynucleosides for the synthesis of DNA fragments simplifying deprotection and isolation of the final product," *Nucleic Acids Research*, vol. 12, no. 11, pp. 4539–4557, Jun. 1984. [Online]. Available: https://doi.org/10.1093/nar/12.11.4539

[31] C. H. Paul and A. T. Royappa, "Acid Binding and Detritylation During Oligonucleotide Synthesis," *Nucleic Acids Research*, vol. 24, no. 15, pp. 3048–3052, Aug. 1996. [Online]. Available: https://doi.org/10.1093/nar/24.15.3048

[32] D. C. Capaldi, A. N. Scozzari, D. L. Cole, and V. T. Ravikumar, "Is It Essential to Use Anhydrous Acetonitrile in the Manufacture of Phosphorothioate Oligonucleotides?" *Organic Process Research & Development*, vol. 3, no. 6, pp. 485–487, Nov. 1999, publisher: American Chemical Society. [Online]. Available: https://doi.org/10.1021/op9900333

[33] M. Sekine, "DNA Synthesis Without Base Protection," *Current Protocols in Nucleic Acid Chemistry*, vol. 18, no. 1, pp. 3.10.1–3.10.15, 2004, _-eprint: https://onlinelibrary.wiley.com/doi/pdf/10.1002/0471142700.nc0310s18. [Online]. Available: http://currentprotocols.onlinelibrary.wiley.com/doi/abs/10.1002/0471142700.nc0310s18

[34] A. R. Wheeler, H. Moon, C.-J. . Kim, J. A. Loo, and R. L. Garrell, "Electrowetting-Based Microfluidics for Analysis of Peptides and Proteins by Matrix-Assisted Laser Desorption/Ionization Mass Spectrometry," *Analytical Chemistry*, vol. 76, no. 16, pp. 4833–4838, Aug. 2004, publisher: American Chemical Society. [Online]. Available: https://doi.org/10.1021/ac0498112

[35] W. C. Nelson, I. Peng, G.-A. Lee, J. A. Loo, R. L. Garrell, and C.-J. CJ Kim, "Incubated Protein Reduction and Digestion on an Electrowetting-on-Dielectric Digital Microfluidic Chip for MALDI-MS," *Analytical Chemistry*, vol. 82, no. 23, pp. 9932–9937, Dec. 2010, publisher: American Chemical Society. [Online]. Available: https://doi.org/10.1021/ac101833b

[36] Y. Li, R. J. Baker, and D. Raad, "Improving the performance of electrowetting on dielectric microfluidics using piezoelectric top plate control," *Sensors and Actuators B: Chemical*, vol. 229, pp. 63–74, Jun. 2016. [Online]. Available: http://www.sciencedirect.com/science/article/pii/S0925400516301083

[37] W.-H. Chen, Z.-J. Qin, J. Wang, and G.-P. Zhao, "The MASTER (methylation-assisted tailorable ends rational) ligation method for seamless DNA assembly," *Nucleic Acids Research*, vol. 41, no. 8, pp. e93–e93, Apr. 2013, publisher: Oxford Academic. [Online]. Available: https://academic.oup.com/nar/article/41/8/e93/2409141

[38] S. d. Kok, L. H. Stanton, T. Slaby, M. Durot, V. F. Holmes, K. G. Patel, D. Platt, E. B. Shapland, Z. Serber, J. Dean, J. D. Newman, and S. S. Chandran, "Rapid and Reliable DNA Assembly via Ligase Cycling Reaction," *ACS Synthetic Biology*, vol. 3, no. 2, pp. 97–106, Feb. 2014, publisher: American Chemical Society. [Online]. Available: https://doi.org/10.1021/sb4001992

[39] R. B. Fair, "Digital microfluidics: is a true lab-on-a-chip possible?" *Microfluidics and Nanofluidics*, vol. 3, no. 3, pp. 245–281, Apr. 2007. [Online]. Available: http://link.springer.com/10.1007/s10404-007-0161-8

[40] M. Washizu, "Electrostatic actuation of liquid droplets for micro-reactor applications," *IEEE Transactions on Industry Applications*, vol. 34, no. 4, pp. 732–737, Jul. 1998, conference Name: IEEE Transactions on Industry Applications.

[41] P. G. de Gennes, "Wetting: statics and dynamics," *Reviews of Modern Physics*, vol. 57, no. 3, pp. 827–863, Jul. 1985, publisher: American Physical Society. [Online]. Available: https://link.aps.org/doi/10.1103/RevModPhys.57.827

[42] D. Bonn, J. Eggers, J. Indekeu, J. Meunier, and E. Rolley, "Wetting and spreading," *Reviews of Modern Physics*, vol. 81, no. 2, pp. 739–805, May 2009, publisher: American Physical Society. [Online]. Available: https://link.aps.org/doi/10.1103/RevModPhys.81.739

[43] Y. Yuan and T. R. Lee, "Contact Angle and Wetting Properties," in *Surface Science Techniques*, ser. Springer Series in Surface Sciences, G. Bracco and B. Holst, Eds. Berlin, Heidelberg: Springer, 2013, pp. 3–34. [Online]. Available: https://doi.org/10.1007/978-3-642-34243-1_1

[44] W. N. Bond, "The surface tension of a moving water sheet," *Proceedings of the Physical Society*, vol. 47, no. 4, pp. 549–558, Jul. 1935, publisher: IOP Publishing. [Online]. Available: https://doi.org/10.1088/0959-5309/47/4/303

[45] W. H. Hager, "Wilfrid Noel Bond and the Bond number," *Journal of Hydraulic Research*, vol. 50, no. 1, pp. 3–9, Feb. 2012, publisher: Taylor & Francis _eprint: https://doi.org/10.1080/00221686.2011.649839. [Online]. Available: https://doi.org/10.1080/00221686.2011.649839

[46] T. Young, "III. An essay on the cohesion of fluids," *Philosophical Transactions of the Royal Society of London*, vol. 95, pp. 65–87, Jan. 1805. [Online]. Available: https://royalsocietypublishing.org/doi/abs/10.1098/rstl.1805.0005

[47] W. A. ZISMAN, "Relation of the Equilibrium Contact Angle to Liquid and Solid Constitution," in *Contact Angle, Wettability, and Adhesion*, ser. Advances in Chemistry. AMERICAN CHEMICAL SOCIETY, Jan. 1964, vol. 43, no. 43, pp. 1–51, section: 1. [Online]. Available: https://doi.org/10.1021/ba-1964-0043.ch001

[48] G. Whyman, E. Bormashenko, and T. Stein, "The rigorous derivation of Young, CassieBaxter and Wenzel equations and the analysis of the contact angle hysteresis phenomenon," *Chemical Physics Letters*, vol. 450, no. 4, pp. 355–359, Jan. 2008. [Online]. Available: http://www.sciencedirect.com/science/article/pii/S000926140701545X

[49] R. N. Wenzel, "Surface Roughness and Contact Angle." *The Journal of Physical and Colloid Chemistry*, vol. 53, no. 9, pp. 1466–1467, Sep. 1949. [Online]. Available: https://pubs.acs.org/doi/abs/10.1021/j150474a015

[50] J. F. Joanny and P. G. de Gennes, "A model for contact angle hysteresis," *The Journal of Chemical Physics*, vol. 81, no. 1, pp. 552–562, Jul. 1984, publisher: American Institute of Physics. [Online]. Available: http://aip.scitation.org/doi/10.1063/1.447337

[51] C. W. Extrand and Y. Kumagai, "An Experimental Study of Contact Angle Hysteresis," *Journal of Colloid and Interface Science*, vol. 191, no. 2, pp. 378–383, Jul. 1997. [Online]. Available: http://www.sciencedirect.com/science/article/pii/S0021979797949353

[52] L. Gao and T. J. McCarthy, "Contact Angle Hysteresis Explained," *Langmuir*, vol. 22, no. 14, pp. 6234–6237, Jul. 2006, publisher: American Chemical Society. [Online]. Available: https://doi.org/10.1021/la060254j

[53] H. B. Eral, D. J. C. M. t Mannetje, and J. M. Oh, "Contact angle hysteresis: a review of fundamentals and applications," *Colloid and Polymer Science*, vol. 291, no. 2, pp. 247–260, Feb. 2013. [Online]. Available: https://doi.org/10.1007/s00396-012-2796-6

[54] H. J. J. Verheijen and M. W. J. Prins, "Reversible Electrowetting and Trapping of Charge: Model and Experiments," *Langmuir*, vol. 15, no. 20, pp. 6616–6620, Sep. 1999, publisher: American Chemical Society. [Online]. Available: https://doi.org/10.1021/la990548n

[55] J. Berthier, P. Dubois, P. Clementz, P. Claustre, C. Peponnet, and Y. Fouillet, "Actuation potentials and capillary forces in electrowetting based microsystems," *Sensors and Actuators A: Physical*, vol. 134, no. 2, pp. 471–479, Mar. 2007. [Online]. Available: http://www.sciencedirect.com/science/article/pii/S0924424706003268

[56] F. Li and F. Mugele, "How to make sticky surfaces slippery: Contact angle hysteresis in electrowetting with alternating voltage," *Applied Physics Letters*, vol. 92, no. 24, p. 244108, Jun. 2008, publisher: American Institute of Physics. [Online]. Available: http://aip.scitation.org/doi/full/10.1063/1.2945803

[57] W. C. Nelson, P. Sen, and C.-J. . Kim, "Dynamic Contact Angles and Hysteresis under Electrowetting-on-Dielectric," *Langmuir*, vol. 27, no. 16, pp. 10319–10326, Aug. 2011, publisher: American Chemical Society. [Online]. Available: https://doi.org/10.1021/la2018083

[58] R. Gupta, D. M. Sheth, T. K. Boone, A. B. Sevilla, and J. Fréchette, "Impact of Pinning of the Triple Contact Line on Electrowetting Performance," *Langmuir*, vol. 27, no. 24, pp. 14 923–14 929, Dec. 2011, publisher: American Chemical Society. [Online]. Available: https://doi.org/10.1021/la203320g

[59] F. Mugele and J.-C. Baret, "Electrowetting: from basics to applications," *Journal of Physics: Condensed Matter*, vol. 17, no. 28, pp. R705–R774, Jul. 2005, publisher: IOP Publishing. [Online]. Available: https://doi.org/10.1088%2F0953-8984%2F17%2F28%2Fr01

[60] G. Lippmann, France, Université (1806-1896), and Faculté des sciences (Paris ; 1806-1896), "Relations entre les phénomènes électriques et capillaires," Ph.D. dissertation, Gauthier-Villars, Paris, 1875, oCLC: 490702474.

[61] A. Quinn, R. Sedev, and J. Ralston, "Contact Angle Saturation in Electrowetting," *The Journal of Physical Chemistry B*, vol. 109, no. 13, pp. 6268–6275, Apr. 2005, publisher: American Chemical Society. [Online]. Available: https://doi.org/10.1021/jp040478f

[62] E. Bormashenko, "Contact Angles of Sessile Droplets Deposited on Rough and Flat Surfaces in the Presence of External Fields," *Mathematical Modelling of Natural Phenomena*, vol. 7, no. 4, pp. 1–5, 2012, publisher: EDP Sciences. [Online]. Available: https://doi.org/10.1051/mmnp/20127401

[63] K. H. Kang, "How Electrostatic Fields Change Contact Angle in Electrowetting," *Langmuir*, vol. 18, no. 26, pp. 10 318–10 322, Dec. 2002, publisher: American Chemical Society. [Online]. Available: https://doi.org/10.1021/la0263615

[64] V. Peykov, A. Quinn, and J. Ralston, "Electrowetting: a model for contact-angle saturation," *Colloid and Polymer Science*, vol. 278, no. 8, pp. 789–793, Aug. 2000. [Online]. Available: https://doi.org/10.1007/s003960000333

[65] A. G. Papathanasiou and A. G. Boudouvis, "Manifestation of the connection between dielectric breakdown strength and contact angle saturation in electrowetting," *Applied Physics Letters*, vol. 86, no. 16, p. 164102, Apr. 2005, publisher: American Institute of Physics. [Online]. Available: http://aip.scitation.org/doi/full/10.1063/1.1905809

[66] H. Liu, S. Dharmatilleke, D. K. Maurya, and A. A. O. Tay, "Dielectric materials for electrowetting-on-dielectric actuation," *Microsystem Technologies*, vol. 16, no. 3, p. 449, Nov. 2009. [Online]. Available: https://doi.org/10.1007/s00542-009-0933-z

[67] A. G. Papathanasiou, A. T. Papaioannou, and A. G. Boudouvis, "Illuminating the connection between contact angle saturation and dielectric breakdown in electrowetting through leakage current measurements," *Journal of Applied Physics*, vol. 103, no. 3, p. 034901, Feb. 2008, publisher: American Institute of Physics. [Online]. Available: http://aip.scitation.org/doi/full/10.1063/1.2837100

[68] F. Mugele, "Fundamental challenges in electrowetting: from equilibrium shapes to contact angle saturation and drop dynamics," *Soft Matter*, vol. 5, no. 18, pp. 3377–3384, 2009, publisher: Royal Society of Chemistry. [Online]. Available: http://pubs.rsc.org/en/content/articlelanding/2009/sm/b904493k

[69] H. A. A. Ali, H. A. Mohamed, and M. Abdelgawad, "Repulsion-based model for contact angle saturation in electrowetting," *Biomicrofluidics*, vol. 9, no. 1, p. 014115, Jan. 2015, publisher: American Institute of Physics. [Online]. Available: http://aip.scitation.org/doi/full/10.1063/1.4907977

[70] A. I. Drygiannakis, A. G. Papathanasiou, and A. G. Boudouvis, "On the Connection between Dielectric Breakdown Strength, Trapping of Charge, and Contact Angle Saturation in Electrowetting," *Langmuir*, vol. 25, no. 1, pp. 147–152, Jan. 2009, publisher: American Chemical Society. [Online]. Available: https://doi.org/10.1021/la802551j

[71] T. Vilkner, D. Janasek, and A. Manz, "Micro Total Analysis Systems. Recent Developments," *Analytical Chemistry*, vol. 76, no. 12, pp. 3373–3386, Jun. 2004, publisher: American Chemical Society. [Online]. Available: https://doi.org/10.1021/ac040063q

[72] H. Stone, A. Stroock, and A. Ajdari, "Engineering Flows in Small Devices: Microfluidics Toward a Lab-on-a-Chip," *Annual Review of Fluid Mechanics*, vol. 36, no. 1, pp. 381–411, 2004, _eprint: https://doi.org/10.1146/annurev.fluid.36.050802.122124. [Online]. Available: https://doi.org/10.1146/annurev.fluid.36.050802.122124

[73] H. Ren, R. B. Fair, M. G. Pollack, and E. J. Shaughnessy, "Dynamics of electro-wetting droplet transport," *Sensors and Actuators B: Chemical*, vol. 87, no. 1, pp. 201–206, Nov. 2002. [Online]. Available: http://www.sciencedirect.com/science/article/pii/S092540050200223X

[74] J. Zeng and T. Korsmeyer, "Principles of droplet electrohydrodynamics for lab-on-a-chip," *Lab on a Chip*, vol. 4, no. 4, pp. 265–277, Jul. 2004, publisher: The Royal Society of Chemistry. [Online]. Available: http://pubs.rsc.org/en/content/articlelanding/2004/lc/b403082f

[75] S. W. Walker and B. Shapiro, "Modeling the fluid dynamics of electrowetting on dielectric (EWOD)," *Journal of Microelectromechanical Systems*, vol. 15, no. 4, pp. 986–1000, Aug. 2006, conference Name: Journal of Microelectromechanical Systems.

[76] E. S. Baird and K. Mohseni, "A Unified Velocity Model for Digital Microfluidics," *Nanoscale and Microscale Thermophysical Engineering*, vol. 11, no. 1-2, pp. 109–120, May 2007, publisher: Taylor & Francis _eprint: https://doi.org/10.1080/15567260701337514. [Online]. Available: https://doi.org/10.1080/15567260701337514

[77] J. H. Song, R. Evans, Y.-Y. Lin, B.-N. Hsu, and R. B. Fair, "A scaling model for electrowetting-on-dielectric microfluidic actuators," *Microfluidics and Nanofluidics*, vol. 7, no. 1, pp. 75–89, Jul. 2009. [Online]. Available: https://doi.org/10.1007/s10404-008-0360-y

[78] M. J. Schertzer, S. I. Gubarenko, R. Ben-Mrad, and P. E. Sullivan, "An Empirically Validated Analytical Model of Droplet Dynamics in Electrowetting on Dielectric Devices," *Langmuir*, vol. 26, no. 24, pp. 19 230–19 238, Dec. 2010, publisher: American Chemical Society. [Online]. Available: https://doi.org/10.1021/la103702t

[79] M. Pollack, A. D.ăShenderov, and R. B.ăFair, "Electrowetting-based actuation of droplets for integrated microfluidics," *Lab on a Chip*, vol. 2, no. 2, pp. 96–101, 2002. [Online]. Available: https://pubs.rsc.org/en/content/articlelanding/2002/lc/b110474h

[80] L.-S. Jang, C.-Y. Hsu, and C.-H. Chen, "Effect of electrode geometry on performance of EWOD device driven by battery-based system," *Biomedical Microdevices*, vol. 11, no. 5, p. 1029, May 2009. [Online]. Available: https://doi.org/10.1007/s10544-009-9320-x

[81] M. Abdelgawad, P. Park, and A. R. Wheeler, "Optimization of device geometry in single-plate digital microfluidics," *Journal of Applied Physics*, vol. 105, no. 9, p. 094506, May 2009, publisher: American Institute of Physics. [Online]. Available: http://aip.scitation.org/doi/full/10.1063/1.3117216

[82] V. Jain, V. Devarasetty, and R. Patrikar, "Effect of electrode geometry on droplet velocity in open EWOD based device for digital microfluidics applications," *Journal of Electrostatics*, vol. 87, pp. 11–18, Jun. 2017. [Online]. Available: https://www.sciencedirect.com/science/article/pii/S0304388616302297

[83] S. K. Cho, H. Moon, and C.-J. Kim, "Creating, transporting, cutting, and merging liquid droplets by electrowetting-based actuation for digital microfluidic circuits," *Journal of Microelectromechanical Systems*, vol. 12, no. 1, pp. 70–80, Feb. 2003.

[84] J. Gong and C.-J. . Kim, "All-electronic droplet generation on-chip with real-time feedback control for EWOD digital microfluidics," *Lab on a Chip*, vol. 8, no. 6, pp. 898–906, May 2008, publisher: The Royal Society of Chemistry. [Online]. Available: http://pubs.rsc.org/en/content/articlelanding/2008/lc/b717417a

[85] M. Yafia and H. Najjaran, "High precision control of gap height for enhancing principal digital microfluidics operations," *Sensors and Actuators B: Chemical*, vol. 186, pp. 343–352, Sep. 2013. [Online]. Available: https://www.sciencedirect.com/science/article/pii/S0925400513007107

[86] Y. Guan, B. Li, and L. Xing, "Numerical investigation of electrowetting-based droplet splitting in closed digital microfluidic system: Dynamics, mode, and satellite droplet," *Physics of Fluids*, vol. 30, no. 11, p. 112001, Nov. 2018, publisher: American Institute of Physics. [Online]. Available: http://aip.scitation.org/doi/full/10.1063/1.5049511

[87] E. Samiei and M. Hoorfar, "Systematic analysis of geometrical based unequal droplet splitting in digital microfluidics," *Journal of Micromechanics and Microengineering*, vol. 25, no. 5, p. 055008, Apr. 2015, publisher: IOP Publishing. [Online]. Available: https://doi.org/10.1088/0960-1317/25/5/055008

[88] N. Y. J. B. Nikapitiya, S. M. You, and H. Moon, "Droplet dispensing and splitting by electrowetting on dielectric digital microfluidics," in *2014 IEEE 27th International Conference on Micro Electro Mechanical Systems (MEMS)*, Jan. 2014, pp. 955–958, iSSN: 1084-6999.

[89] J.-Y. Yoon and R. L. Garrell, "Biomolecular Adsorption in Microfluidics," in *Encyclopedia of Microfluidics and Nanofluidics*, D. Li, Ed. Boston, MA: Springer US, 2013, pp. 1–13. [Online]. Available: https://doi.org/10.1007/978-3-642-27758-0_87-2

[90] E. T. Dimalanta, A. Lim, R. Runnheim, C. Lamers, C. Churas, D. K. Forrest, J. J. de Pablo, M. D. Graham, S. N. Coppersmith, S. Goldstein, and D. C. Schwartz, "A Microfluidic System for Large DNA Molecule Arrays," *Analytical Chemistry*, vol. 76, no. 18, pp. 5293–5301, Sep. 2004, publisher: American Chemical Society. [Online]. Available: https://doi.org/10.1021/ac0496401

[91] Y. Zhang and P. Ozdemir, "Microfluidic DNA amplificationA review," *Analytica Chimica Acta*, vol. 638, no. 2, pp. 115–125, Apr. 2009. [Online]. Available: https://www.sciencedirect.com/science/article/pii/S0003267009003031

[92] V. Gubala, J. Siegrist, R. Monaghan, B. OReilly, R. P. Gandhiraman, S. Daniels, D. E. Williams, and J. Ducrée, "Simple approach to study biomolecule adsorption in polymeric microfluidic channels," *Analytica Chimica Acta*, vol. 760, pp. 75–82, Jan. 2013. [Online]. Available: https://www.sciencedirect.com/science/article/pii/S0003267012017060

[93] R. R. Choudhury, J. M. Gohil, S. Mohanty, and S. K. Nayak, "Antifouling, fouling release and antimicrobial materials for surface modification of reverse osmosis and nanofiltration membranes," *Journal of Materials Chemistry A*, vol. 6, no. 2, pp. 313–333, Jan. 2018, publisher: The Royal Society of Chemistry. [Online]. Available: http://pubs.rsc.org/en/content/articlelanding/2018/ta/c7ta08627j

[94] X. Zhao, R. Zhang, Y. Liu, M. He, Y. Su, C. Gao, and Z. Jiang, "Antifouling membrane surface construction: Chemistry plays a critical role," *Journal of Membrane Science*, vol. 551, pp. 145–171, Apr. 2018. [Online]. Available: https://www.sciencedirect.com/science/article/pii/S0376738817332428

[95] H. Bi, W. Zhong, S. Meng, J. Kong, P. Yang, and B. Liu, "Construction of a Biomimetic Surface on Microfluidic Chips for Biofouling Resistance," *Analytical Chemistry*, vol. 78, no. 10, pp. 3399–3405, May 2006, publisher: American Chemical Society. [Online]. Available: https://doi.org/10.1021/ac0522963

[96] P. Halder, M. Nasabi, F. J. T. Lopez, N. Jayasuriya, S. Bhattacharya, M. Deighton, A. Mitchell, and M. A. Bhuiyan, "A novel approach to determine the efficacy of patterned surfaces for biofouling control in relation to its microfluidic environment," *Biofouling*, vol. 29, no. 6, pp. 697–713, Jul. 2013, publisher: Taylor & Francis _eprint: https://doi.org/10.1080/08927014.2013.800192. [Online]. Available: https://doi.org/10.1080/08927014.2013.800192

[97] G. Perry, V. Thomy, M. R. Das, Y. Coffinier, and R. Boukherroub, "Inhibiting protein biofouling using graphene oxide in droplet-based microfluidic microsystems," *Lab on a Chip*, vol. 12, no. 9, pp. 1601–1604, Apr. 2012, publisher: The Royal Society of Chemistry. [Online]. Available: http://pubs.rsc.org/en/content/articlelanding/2012/lc/c2lc21279j

[98] E. K. U. Larsen and N. B. Larsen, "One-step polymer surface modification for minimizing drug, protein, and DNA adsorption in microanalytical systems," *Lab on a Chip*, vol. 13, no. 4, pp. 669–675, Jan. 2013, publisher: The Royal Society of Chemistry. [Online]. Available: http://pubs.rsc.org/en/content/articlelanding/2013/lc/c2lc40750g

[99] S. H. Au, P. Kumar, and A. R. Wheeler, "A New Angle on Pluronic Additives: Advancing Droplets and Understanding in Digital Microfluidics," *Langmuir*, vol. 27, no. 13, pp. 8586–8594, Jul. 2011, publisher: American Chemical Society. [Online]. Available: https://doi.org/10.1021/la201185c

[100] J. Kleinert, V. Srinivasan, A. Rival, C. Delattre, O. D. Velev, and V. K. Pamula, "The dynamics and stability of lubricating oil films during droplet transport by electrowetting in microfluidic devices," *Biomicrofluidics*, vol. 9, no. 3, p. 034104, May 2015, publisher: American Institute of Physics. [Online]. Available: http://aip.scitation.org/doi/full/10.1063/1.4921489

[101] H. Geng and S. K. Cho, "Antifouling digital microfluidics using lubricant infused porous film," *Lab on a Chip*, vol. 19, no. 13, pp. 2275–2283, Jun. 2019, publisher: The Royal Society of Chemistry. [Online]. Available: http://pubs.rsc.org/en/content/articlelanding/2019/lc/c9lc00289h

[102] R. A. Hughes, A. E. Miklos, and A. D. Ellington, "Chapter twelve - Gene Synthesis: Methods and Applications," in *Methods in Enzymology*, ser. Synthetic Biology, Part B, C. Voigt, Ed. Academic Press, Jan. 2011, vol. 498, pp. 277–309. [Online]. Available: http://www.sciencedirect.com/science/article/pii/B9780123851208000127

[103] H. O. Smith, C. A. Hutchison, C. Pfannkoch, and J. C. Venter, "Generating a synthetic genome by whole genome assembly: X174 bacteriophage from synthetic oligonucleotides," *Proceedings of the National Academy of Sciences*, vol. 100, no. 26, pp. 15 440–15 445, Dec. 2003, iSBN: 9782237126104 Publisher: National Academy of Sciences Section: Biological Sciences. [Online]. Available: https://www.pnas.org/content/100/26/15440

[104] D. R. Horspool, R. J. Coope, and R. A. Holt, "Efficient assembly of very short oligonucleotides using T4 DNA Ligase," *BMC Research Notes*, vol. 3, no. 1, p. 291, Nov. 2010. [Online]. Available: https://doi.org/10.1186/1756-0500-3-291

[105] J. C. Klein, M. J. Lajoie, J. J. Schwartz, E.-M. Strauch, J. Nelson, D. Baker, and J. Shendure, "Multiplex pairwise assembly of array-derived DNA oligonucleotides," *Nucleic Acids Research*, vol. 44, no. 5, pp. e43–e43, Mar. 2016. [Online]. Available: https://doi.org/10.1093/nar/gkv1177

[106] M. J. Schertzer, R. Ben-Mrad, and P. E. Sullivan, "Mechanical Filtration of Particles in Electrowetting on Dielectric Devices," *Journal of Microelectromechanical Systems*, vol. 20, no. 4, pp. 1010–1015, Aug. 2011, conference Name: Journal of Microelectromechanical Systems.

[107] N. Y. Jagath, B. Nikapitiya, S. M. You, and H. Moon, "Droplet dispensing and splitting by electrowetting on dielectric digital microfluidics," in *2014 IEEE 27th International Conference on Micro Electro Mechanical Systems (MEMS)*, Jan. 2014, pp. 955–958, iSSN: 1084-6999.

[108] V. Srinivasan, V. K. Pamula, and R. B. Fair, "An integrated digital microfluidic lab-on-a-chip for clinical diagnostics on human physiological fluids," *Lab on a Chip*, vol. 4, no. 4, pp. 310–315, Jul. 2004, publisher: The Royal Society of Chemistry. [Online]. Available: http://pubs.rsc.org/en/content/articlelanding/2004/lc/b403341h

[109] D. Brassard, L. Malic, F. Normandin, M. Tabrizian, and T. Veres, "Water-oil core-shell droplets for electrowetting-based digital microfluidic devices," *Lab on a Chip*, vol. 8, no. 8, pp. 1342–1349, Jul. 2008, publisher: The Royal Society of Chemistry. [Online]. Available: http://pubs.rsc.org/en/content/articlelanding/2008/lc/b803827a

[110] Y.-H. Chang, G.-B. Lee, F.-C. Huang, Y.-Y. Chen, and J.-L. Lin, "Integrated polymerase chain reaction chips utilizing digital microfluidics," *Biomedical Microdevices*, vol. 8, no. 3, pp. 215–225, Sep. 2006. [Online]. Available: https://doi.org/10.1007/s10544-006-8171-y

[111] R. Fobel, C. Fobel, and A. R. Wheeler, "DropBot: An open-source digital microfluidic control system with precise control of electrostatic driving force and instantaneous drop velocity measurement," *Applied Physics Letters*, vol. 102, no. 19, p. 193513, May 2013, publisher: American Institute of Physics. [Online]. Available: http://aip.scitation.org/doi/full/10.1063/1.4807118

[112] P. Paik, V. K. Pamula, and R. B. Fair, "Rapid droplet mixers for digital microfluidic systems," *Lab on a Chip*, vol. 3, no. 4, pp. 253–259, Nov. 2003, publisher: The Royal Society of Chemistry. [Online]. Available: http://pubs.rsc.org/en/content/articlelanding/2003/lc/b307628h

[113] J. Fowler, Hyejin Moon, and Chang-Jin Kim, "Enhancement of mixing by droplet-based microfluidics," in *Technical Digest. MEMS 2002 IEEE International Conference. Fifteenth IEEE International Conference on Micro Electro Mechanical Systems (Cat. No.02CH37266)*, Jan. 2002, pp. 97–100, iSSN: 1084-6999.

[114] H. T. An, S. Houchaimi, C. T. Burkhart, and M. J. Schertzer, "DNA Ligation on a Digital Microfluidic Device." American Society of Mechanical Engineers Digital Collection, Oct. 2020. [Online]. Available: http://journals.asmedigitalcollection.asme.org/ICNMM/proceedings/ICNMM2020/83693/V001T12A004/1088214

Appendix A   DMFL Shared Repository

The DMFL shared google drive contains all the files necessary to recreate this work. This repository contains files such as device layouts, device fabrication process flows, LabVIEW virtual instruments, thesis documents and images, and device testing videos.

Appendix B   DMF Device Fabrication Process

Details regarding the fabrication process for the final DMF devices used in this thesis work are provided as reference. This fabrication process can be found in the shared DMFL file repository. DMF device fabrication was conducted using conventional tools and materials in the RIT SMFL. The DMF chip is fabricated using the entirety of this process while the top plate only uses the Teflon spin coat and cure.

Level 1 Lithography:

1. Perform an O2 plasma surface enhancement on device slides by placing in the LAM 490 on a carrier wafer with the following recipe:
   - Step 1: 300 mTorr, 000 W, 100 sccm of O2, 1 min
   - Step 2: 300 mTorr, 100 W, 100 sccm of O2, 30 sec
   - Step 3: 300 mTorr, 0 sec
2. Perform a dehydration bake at 120řC for 60 sec and cool on heatsink.
3. Coat wafers using the CEE Resist Spinner with AZ MIR 701 i-line positive photoresist using Program #0.
4. Conduct a post application bake at 90řC for 60 sec and cool on heatsink.
5. Prepare the Suss MA150 Contact Aligner by measuring and recording the irradiance of the exposure.
6. Using the equation D = I * t, calculate and record the appropriate time to achieve a dose of 300 mJ/cm2.
7. Conduct a post exposure bake at 110řC for 60 sec and cool on heatsink.
8. Using the CEE Resist Developer, develop the substrates using Program #0. MAKE SURE THE DEVELOPER COVERS THE ENTIRE WAFER!
9. Conduct a hard bake at 140řC for 60 sec and cool on heatsink.

Aluminum Etch & Solvent Strip:

1. Place the substrates into the only 3 in substrate Teflon boat.
2. Start heating the Al Etch & Solvent Strip bench (Takes approximately 15 45 min).
3. Etch the substrates for at least 5 min.
4. Rinse substrates for 5 min.
5. Rinse and dry one device at Manual Chemistry Bench.
6. Inspect same device under microscope around dense traces to check for shorts or open circuits. Adjust etch times accordingly.
7. Rinse and thoroughly dry individually on Manual Chemistry Bench.
8. Strip the photoresist for at least 5 min in first bath and 5 min in the second bath.
9. Rinse substrates for 5 min.
10. Rinse and thoroughly dry individually on Manual Chemistry Bench.
11. Measure aluminum thickness using the Tencor P2 Profilometer.

Level 2 Lithography:

1. Perform an O2 plasma surface enhancement on device slides by placing in the LAM 490 on a carrier wafer with the following recipe:

    - Step 1: 300 mTorr, 000 W, 100 sccm of O2, 1 min
    - Step 2: 300 mTorr, 100 W, 100 sccm of O2, 30 sec
    - Step 3: 300 mTorr, 0 sec

2. Conduct a dehydration bake at 120řC for 60 sec cool on heatsink.
3. Coat devices using the SCS Spin Coater with SU-8 3050 i-line negative photoresist using a custom program with the following parameters:

    - RPM 1 - 1500 RPM
    - RAMP 1 - 20 sec
    - TIME 1 - 10 sec
    - RPM 2 - 4000 RPM
    - RAMP 2 - 10 sec
    - TIME 2 - 30 sec

4. Conduct a post application bake at 95řC for 2 min and cool on heatsink.
5. Prepare the Suss MA150 Contact Aligner by measuring and recording the irradiance of the exposure. MASK IS FOIL, MAKE SURE TO ALIGN WELL TO EXPOSE MIDDLE OF DEVICE AND COVER CONNECTION POINTS.
6. Using the equation D = I * t, calculate and record the appropriate time to achieve a dose of 150 mJ/cm2.
7. Conduct a post exposure bake at 65řC for 60 sec and cool on heatsink.
8. Conduct a second post exposure bake at 95řC for 60 sec and cool on heatsink.
9. On a Manual Chemistry Bench, using SU-8 Developer and Isopropyl Alcohol, develop the substrates for 2 min with good agitation, spray a puddle of fresh developer for 15 sec, and rinse both sides of the wafer thoroughly with IPA.
10. Dry the substrate with a Nitrogen gun until visibly dry.
11. Conduct a ramped hard bake by placing on a cool hot plate, setting to 175řC, and baking for 5 min once temperature is reached. Cool on heatsink.

12. Measure the SU-8 thickness using the Tencor P2 Profilometer.
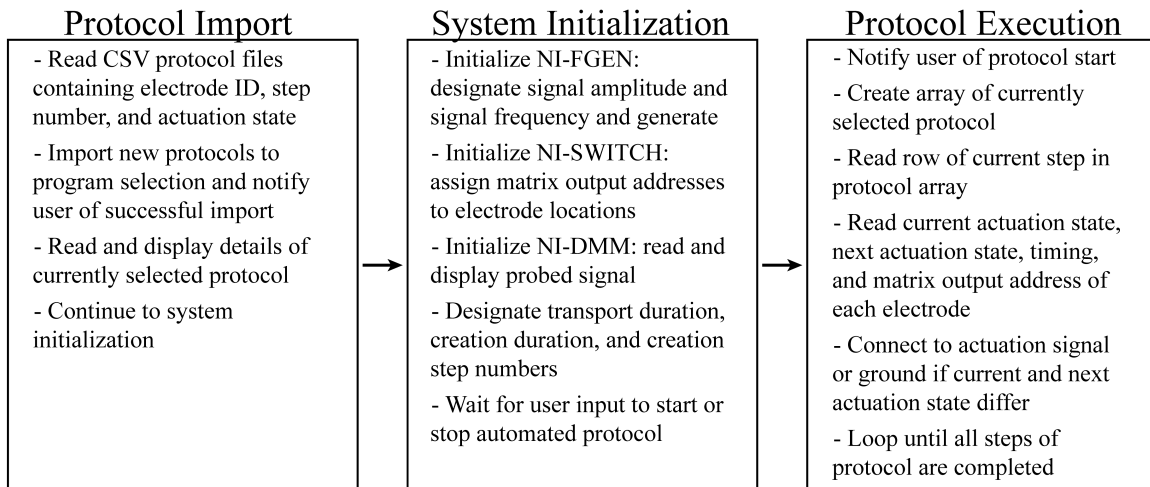

Level 3 Lithography:

1. Perform an O2 plasma surface enhancement on device slides by placing in the LAM 490 on a carrier wafer with the following recipe:

   - Step 1: 300 mTorr, 000 W, 100 sccm of O2, 1 min
   - Step 2: 300 mTorr, 100 W, 100 sccm of O2, 30 sec
   - Step 3: 300 mTorr, 0 sec

2. Conduct a prebake at 65řC for 1 min.
3. Conduct a ramped dehydration bake on previous hot plate, setting to 120řC, and baking for 15 min once temperature is reached. Let cool on hot plate after turning off.
4. Coat devices using the SCS Spin Coater with SU-8 2100 i-line negative photoresist using a custom program with the following parameters:

   - RPM 1 - 500 RPM
   - RAMP 1 - 5 sec
   - TIME 1 - 10 sec
   - RPM 2 - 3000 RPM
   - RAMP 2 - 15 sec
   - TIME 2 - 45 sec

5. Conduct a prebake at 65řC for 5 min.
6. Conduct a ramped post application bake on previous hot plate, setting to 95řC, and baking for 25 min once temperature is reached. Cool on heatsink.
7. Prepare the Suss MA150 Contact Aligner by measuring and recording the irradiance of the exposure.
8. Using the equation D = I * t, calculate and record the appropriate time to achieve a dose of 300 mJ/cm2.
9. Conduct a prebake at 65řC for 5 min.
10. Conduct a ramped post exposure bake on previous hot plate, setting to 85řC, and baking for 15 min once temperature is reached. Cool on heatsink.
11. On a Manual Chemistry Bench, using SU-8 Developer and Isopropyl Alcohol, develop the substrates for 13 min with good agitation, spray a puddle of fresh developer for 15 sec, and rinse both sides of the wafer thoroughly with IPA.
12. Dry the substrate with a Nitrogen gun until visibly dry.
13. Conduct a ramped hard bake on a cool hot plate, setting to 160řC, and baking for 30 min once temperature is reached. Let cool on hot plate after turning off.
14. Measure the SU-8 thickness using the Tencor P2 Profilometer.

Teflon Spin Coat and Cure:

1. Perform an O2 plasma surface enhancement by placing in the LAM 490 with the following recipe:

    - Step 1: 300 mTorr, 000 W, 100 sccm of O2, 1 min
    - Step 2: 300 mTorr, 100 W, 100 sccm of O2, 30 sec
    - Step 3: 300 mTorr, 0 sec

2. Conduct a dehydration bake at 120řC for 60 sec cool on heatsink.
3. Fully cover the Aluminum electrodes using Kapton tape
4. Coat wafers using the SCS Coater with Fluorinert diluted Teflon (2%) using a custom program with the following parameters:

    - RPM 1 - 1500 RPM
    - RAMP 1 - 10 sec
    - TIME 1 - 60 sec

5. Conduct a ramped hard bake on a cool hot plate, setting to 180řC, and baking for 10 min once temperature is reached. Let cool on hot plate after turning off.
6. Remove the Kapton tape with care.
7. Inspect the final device on microscope at critical features.

Appendix C   LabVIEW Virtual Instrument

Details regarding the custom LabVIEW virtual instrument (vi) used to control DMF device prototypes are provided as a reference. The custom VI can be found in the shared DMF file repository. This VI consists of a block diagram and front panel. Programming of the VI is done in the block diagram using symbols, objects, and boolean logic. Various parameters, settings, and controls in the front panel are tied to symbols in the block diagram. This VI follows a sequence of protocol import, system initialization, and protocol execution. The details of each portion of the VI can be seen in Figure C.1.

Protocol Import

- Read CSV protocol files containing electrode ID, step number, and actuation state
- Import new protocols to program selection and notify user of successful import
- Read and display details of currently selected protocol
- Continue to system initialization

System Initialization

- Initialize NI-FGEN: designate signal amplitude and signal frequency and generate
- Initialize NI-SWITCH: assign matrix output addresses to electrode locations
- Initialize NI-DMM: read and display probed signal
- Designate transport duration, creation duration, and creation step numbers
- Wait for user input to start or stop automated protocol

Protocol Execution

- Notify user of protocol start
- Create array of currently selected protocol
- Read row of current step in protocol array
- Read current actuation state, next actuation state, timing, and matrix output address of each electrode
- Connect to actuation signal or ground if current and next actuation state differ
- Loop until all steps of protocol are completed

Figure C.1: Summary of custom LabVIEW virtual instrument programming and execution logic

75